

Investigation of the mechanisms of taxane-induced peripheral neuropathy focusing on Schwann cell and search for novel therapies by drug repositioning

2021

Madoka Koyanagi

Table of contents

Preface	1
Chapter 1: Taxane-induced dedifferentiation of mature myelin-forming Schwann cells participates in CIPN development	
Introduction.....	3
Materials and Methods.....	4
Results.....	11
Discussion.....	17
Chapter 2: Schwann cell-derived galectin-3 has pro-nociceptive roles in taxane-induced peripheral neuropathy	
Introduction.....	20
Materials and Methods.....	21
Results.....	26
Discussion.....	38
Chapter 3: Cilostazol is a causal therapy for preventing taxane-related CIPN by suppression of Schwann cell dedifferentiation	
Introduction.....	42
Materials and Methods.....	43
Results.....	46
Discussion.....	55
Summary	58
Acknowledgements.....	59
List of Publications.....	61
References.....	62

Preface

Taxanes (paclitaxel and docetaxel) are effective first-line chemotherapy agents. However, more than 50% of patients receiving taxanes develop a dose-limiting side effect, chemotherapy-induced peripheral neuropathy (CIPN) (1,2). Symptoms include paresthesia, dysesthesia, numbness, loss of balance, and muscle weakness (3). CIPN is a serious impediment to effective cancer treatment because aggravation of its symptoms results in discontinuation of taxane treatment or dose reduction (4).

Based on the early morphological studies using animal models of CIPN, it has been considered that the direct impairment of peripheral sensory neurons should be a major mechanism for the pathogenesis of CIPN (5-7). However, these notions are insufficient to explain the complex machineries underlying taxane-related CIPN pathogenesis, so that there is no causal therapy to prevent or relieve CIPN (8-10). To address this issue, I focused on Schwann cells, the myelinating glial cells in the peripheral nervous system (PNS).

In Chapter 1, I showed for the first time that treatment with paclitaxel induces the dedifferentiation of myelin-forming Schwann cells prior to impairment of sensory neurons. The data suggest that the direct effects of taxanes on Schwann cells might be the underlying cause of CIPN.

Next, in Chapter 2, I found that galectin-3, a β -galactoside binding protein, was up-regulated in dedifferentiated Schwann cells, and secreted into the culture medium after taxane treatment. Elevation of plasma galectin-3 level was observed in both taxane-treated breast cancer patients with CIPN and a mouse model of taxane-related CIPN. I further confirmed that galectin-3 derived from dedifferentiated Schwann cells plays an important role in the development of taxane-induced mechanical hypersensitivity through chemoattraction of macrophages into the peripheral nerve.

Finally, in Chapter 3, I performed the screening of approved drugs, and consequently, found that a phosphodiesterase (PDE) 3 inhibitor, cilostazol, strongly promoted differentiation of primary cultures of rat Schwann cells. Cilostazol potently inhibited paclitaxel-induced dedifferentiation of Schwann cells, and attenuated the mechanical hypersensitivity in a mouse model of paclitaxel-related CIPN.

These results are described in detail below.

Abbreviations

ANOVA	analyses of variance
BM	bone marrow
cAMP	cyclic adenosine monophosphate
cDNA	complementary deoxyribonucleic acid
CIPN	chemotherapy-induced peripheral neuropathy
CNS	central nervous system
DMSO	dimethyl sulfoxide
DRG	dorsal root ganglia
ELISA	enzyme-linked immunosorbent assay
Epac	exchange protein directly activated by cAMP
GAPDH	glyceraldehyde 3-phosphate dehydrogenase
GFAP	glial fibrillary acidic protein
GFP	green fluorescent protein
HRP	horseradish peroxidase
Iba1	ionized calcium binding adapter molecule 1
IL	interleukin
iNOS	inducible nitric oxide synthase
i.p.	intraperitoneal(ly)
IR	immunoreactivity
IRF	interferon regulatory factor
LVV	lentiviral vector
MAP2	microtubule-associated protein-2
MBP	myelin basic protein
MS	multiple sclerosis
MTT	3-(4,5-dimethylthiazol-2-yl)-2,5-diphenyltetrazolium bromide
NF- κ B	nuclear factor- κ B
NGF	nerve growth factor
OPC	oligodendrocyte precursor cell
PB	phosphate buffer
PBMC	peripheral blood mononuclear cells
PBS	phosphate buffer saline
PCR	polymerase chain reaction
PDE	phosphodiesterase
PLL	poly-L-lysine
PNS	peripheral nervous system
rGalectin-3	recombinant galectin-3
RNA	ribonucleic acid
RT-PCR	reverse transcription-polymerase chain reaction
PVDF	polyvinylidene difluoride
SDS	sodium dodecyl sulfate
TBS	tris-buffered saline
TNF α	tumor necrosis factor- α
WT	wild-type

Chapter 1: Taxane-induced dedifferentiation of mature myelin-forming Schwann cells participates in CIPN development

Introduction

Several animal models of CIPN have been developed to examine the causal mechanisms. Early morphological studies have provided evidence that paclitaxel induces distal axonopathy after systemic administration at relatively high doses or after local injection directly into a peripheral nerve (5,11). Based on these results, taxane-induced peripheral neuropathy has been believed to be secondary to inhibition of the dynamic disassembly of microtubules via binding of taxane to β -tubulin, resulting in a progressive distal axonopathy (6,7,12). However, a growing body of evidence has suggested an alternative hypothesis (13,14). For example, electron microscopic studies of rat peripheral nerves show that treatment with low dose paclitaxel causes a painful peripheral neuropathy, but fails to induce axonal degeneration in peripheral nerves.

Schwann cells are peripheral nervous system glial cells that form a thin myelin sheet by tightly wrapping around axons to enable rapid saltatory conduction of action potentials (15). Schwann cells play a crucial role in the outgrowth and guidance of regrowing peripheral axons after injury. Immediately after peripheral nerve injury, Schwann cells in the injured area transdifferentiate and migrate to the distal end to form a denervated Schwann cell band (16,17). The growth cone of a regrowing peripheral nerve fiber advances toward its original target using the Schwann cells as a guide. Thus, Schwann cells play a major supportive role in the maintenance of the peripheral nervous system, raising the intriguing possibility that impairment of Schwann cells and consequent disruption of intercellular interactions between myelin-forming mature Schwann cells and axons by anti-cancer agents may be important for the pathogenesis of CIPN. Based on this hypothesis, I examined the direct effect of taxanes (paclitaxel and docetaxel) on primary Schwann cell cultures and on myelin-forming Schwann cells in the mouse sciatic nerve.

In this chapter, I show that treatment with taxanes preferentially induce the dedifferentiation of myelin-forming Schwann cells compared to impairment of dorsal root ganglia (DRG) neurons. The present data suggest that the direct effects of taxanes on Schwann cells might be a trigger of CIPN pathogenesis.

Materials and Methods

Animals

All animal experiments were approved by the Kyoto University Animal Research Committee and performed according to the guidelines of the animal ethics committee of Kyoto University. Pregnant Wistar/ST rats, male Wistar/ST rats (6–8 weeks) and male C57BL/6J JmsSlc (5–7 weeks) were obtained from Japan SLC (Shizuoka, Japan). All animals were housed under a 12 h light-dark cycle at a constant ambient temperature ($24 \pm 1^\circ\text{C}$) and humidity ($55 \pm 10\%$), and allowed access to food and water *ad libitum*.

Reagents

Paclitaxel (Sigma-Aldrich, MO, USA; 100 μM) and docetaxel (Wako Pure Chemical Industries, Osaka, Japan; 1mM) were prepared in dimethyl sulfoxide (DMSO, Nacalai Tesque, Kyoto, Japan) and stored at -80°C . Each drug solution was diluted in the appropriate culture medium to achieve the desired concentration before use.

Primary culture of Schwann cells and treatment with anti-cancer agent

Primary Schwann cells were obtained from the sciatic nerves of neonatal Wistar/ST rats (P2–3). The harvested nerves were digested for 1 h at 37°C in culture medium (serum-free Advanced DMEM/F-12; Thermo Fisher Scientific, MA, USA, supplemented with 0.292 mg/ml L-glutamine and 1% penicillin–streptomycin; Nacalai Tesque) containing 250 U/ml hyaluronidase type I-S and 160 U/ml collagenase type I (Sigma-Aldrich). After digestion, tissue fragments were triturated, and the cells were resuspended in maintenance medium (culture medium containing 2 μM forskolin [Sigma-Aldrich] and supplemented with 20 ng/ml heregulin β -1 [Sigma-Aldrich]), and then cultured on a 100 mm culture dish coated with 0.1 mg/ml poly-L-lysine (PLL; Sigma-Aldrich). After 2 days of culture, Schwann cells were purified by magnetic activated cell separation (MACS; Miltenyi Biotec, Germany) using a monoclonal antibody against p75 neurotrophin receptor (Merck, Germany, #MAB365). After 2 days, contaminating fibroblasts were removed by complement-mediated cytolysis using anti-Thy1 antibody (Bio-Rad Laboratories, CA, USA, #MCA02RT) and rabbit complement (MP Biomedicals, CA, USA). Purified immature Schwann cells were then cultured under standard conditions (in maintenance medium) on tissue culture dishes pre-coated with PLL. After 4–7 days of purification, to induce differentiation of Schwann cells, the cells were cultured on PLL and laminin

(Thermo Fisher Scientific)-coated plates (Greiner Bio One International GmbH, Austria) or dishes (Corning Incorporated, NY, USA), and culture medium was replaced with differentiation medium (serum-free Advanced DMEM/F-12, containing 1% penicillin–streptomycin, 0.292 mg/ml L-glutamine, 20 μ M forskolin, and 20 ng/ml heregulin β -1). After 2 days of culture in differentiation medium, Schwann cells were treated with paclitaxel (10 nM), docetaxel (10 nM), or vehicle (0.1% DMSO) for 48 h.

Primary culture of DRG neurons from adult rats

After male rats (6–8 weeks old) were decapitated under deep anesthesia with 3% isoflurane (Nacalai Tesque), the DRG were quickly harvested using forceps. Next, dissected DRG were transferred into a tube containing 1 ml of Hank's balanced salt solution supplemented with 0.3% collagenase type II and 0.4% dispase II (Thermo Fisher Scientific) and incubated for 1 h at 37°C with gentle shaking. After incubation, cells were mechanically dissociated using a pipette. DRG neurons were purified by Percoll (Sigma-Aldrich) density gradient centrifugation. Percoll solutions (30% and 70%) were prepared in L-15 medium (Thermo Fisher Scientific). A Percoll gradient was constructed by layering 3 ml of each Percoll solution into a centrifuge tube. Finally, 1 ml of DRG cell suspension was placed on top of the gradient and centrifuged at $1,800 \times g$ for 15 min at room temperature. Intermediate fractions between each Percoll solution were collected. After washing, cells were re-suspended in Neurobasal medium (Thermo Fisher Scientific) containing 2% B-27 supplement (Thermo Fisher Scientific), 2 mM L-glutamine, 1% penicillin–streptomycin, and 50 ng/ml nerve growth factor (NGF) 2.5S (Sigma-Aldrich). Purified DRG neuronal cells were cultured for 10 days on PLL/laminin-coated coverslips (Fisherbrand Microscope Cover Glass, Thermo Fisher Scientific) in Neurobasal medium.

Co-culture of Schwann cells and DRG neurons

Schwann cell/DRG neuron co-cultures were prepared as described previously (18). Briefly, DRG were dissected from embryonic day 15 Wistar/ST rat pups. The cells were resuspended in MACS neuro medium (Miltenyi Biotec) containing 2% MACS Neuro Brew-21 (Miltenyi Biotec), 0.5% GlutaMAX (Thermo Fisher Scientific), 1% penicillin–streptomycin, and 100 ng/mL 2.5 S NGF, and plated (1.5×10^5 cells per well) in 24-well plates coated with 0.1 mg/mL PLL and 12.5 μ g/mL laminin. Non-neuronal cells were removed by treating the cultures with medium containing 5-fluorodeoxyuridine (FdUr)

(Sigma-Aldrich). After the neural axons grew and expanded, purified Schwann cells (3×10^5 cells per well) were then plated onto established neuronal cultures in DMEM supplemented with 10% FBS and 100 ng/ml 2.5S NGF. Ten days later, the mixed culture of Schwann cells and neurons was treated with 50 μ g/ml ascorbic acid (Sigma-Aldrich) to induce myelination.

Reverse transcription-polymerase chain reaction (RT-PCR) assay

Total RNA was extracted from Schwann cells using the SV Total RNA Isolation system (Promega, WI, USA), according to the manufacturer's instructions. To prepare first strand cDNA, 0.2–1.0 μ g of RNA was incubated in 40 μ l of buffer containing a dNTP mixture, a RT random primer, and reverse transcriptase (High Capacity cDNA Reverse Transcription Kit, Thermo Fisher Scientific), according to the manufacturer's instructions. Each target gene was amplified in a 50 μ l PCR solution containing 2 mM $MgCl_2$, 0.2 mM dNTP mix, and DNA polymerase (Blend Taq[®], TOYOBO, Osaka, Japan) along with synthesized primers targeting *MBP* (sense: 5'-GAA GCC AGG ATT TGG CTA CG-3', antisense: 5'-CAG AGC GGC TGT CTC TTC CT-3'; designed according to GenBank[™] sequence accession number NM_001025291), *p75* (sense: 5'-GCT GGG TTA CCA GCC TGA AC-3', antisense: 5'-GCA GTG GAC TCG CTG CAT AG-3'; designed according to GenBank[™] sequence accession number NM_012610), and glyceraldehyde 3-phosphate dehydrogenase (*GAPDH*, sense: 5'-GTT ACC AGG GCT GCC TTC TC-3', antisense: 5'-TGA TGA CCA GCT TCC CAT TC-3'; designed according to GenBank[™] sequence accession number NM_017008). Samples were heated to 94°C for 2.5 min, 55°C for 30 sec, and 72°C for 1 min and cycled 30 times through 94°C for 30 sec, 55°C for 30 sec, and 72°C for 1 min, with a final extension step at 72°C for 3 min. The mixture was run on 1.5% agarose gels with the indicated markers (TOYOBO). The agarose gel was stained with ethidium bromide (Nacalai Tesque) and photographed under UV transillumination (PhotoDoc-It[™] Imaging System, Analytik Jena AG, Germany).

Viability of Schwann cells

The plated cells were incubated at 37°C for 45 min in 3-(4,5-dimethylthiazol-2-yl)-2,5-diphenyltetrazolium bromide (MTT, Nacalai Tesque) solution (final concentration of 0.05 mg/ml). The medium was then removed, and the purple formazan crystals were dissolved in 150 μ l of DMSO. An aliquot of 100 μ l was extracted from each well and transferred to

96 well plates. The absorbance was then measured in a micro-plate reader (MAXline, Molecular Devices, CA, USA) at 560/630 nm. Cell viability was expressed as the absorbance value of drug-treated groups $\times 100$ / the absorbance value of the vehicle-treated group.

Immunocytochemical analysis of cultured cells

After differentiation or drug treatment, the culture medium was removed and the cells were washed with phosphate buffer saline (PBS) and fixed with 4% paraformaldehyde in PBS for 20 min at room temperature. Cells were washed three times with PBS, blocked, and permeabilized for 30 min in 3% BSA in PBS containing 0.1% Tween 20. Consecutively, cells were incubated with rat anti-myelin basic protein (MBP, 1:250, Merck), mouse anti-p75 (1:500, Merck), rabbit anti-microtubule-associated protein-2 (MAP2, 1:500, Merck), or rabbit anti-p75 (1:500, Abcam) primary antibodies overnight at 4°C. After washing three times with PBS, cells were incubated for 2 h at room temperature with appropriate secondary antibodies conjugated to Alexa Fluor™ 594 and/or Alexa Fluor™ 488 (1:200, Thermo Fisher Scientific). After washing, cultures were mounted using Vectashield containing DAPI (Vector Laboratories, Burlingame, CA, USA) and images were acquired under a laser scanning confocal microscope (Fluoview FV10i; Olympus Corporation, Tokyo, Japan, or A1RMP; Nikon Corporation, Tokyo, Japan).

Western blotting

Schwann cells were homogenized in RIPA-lysing buffer (50 mM Tris-HCl buffer (pH 7.6), 150 mM NaCl, 1% Nonidet P-40, 0.5% sodium deoxycholate, protease inhibitor cocktail (Nacalai Tesque), and 0.1% sodium dodecyl sulfate (SDS)) using a sonicator (Qsonica, CT, USA) and then centrifuged at $1000 \times g$ at 4°C for 10 min. The supernatants were collected, and protein concentrations were determined using a BCA Protein Assay Kit (Thermo Fisher Scientific). An aliquot of supernatant was diluted in NuPAGE® LDS sample buffer (Thermo Fisher Scientific), and proteins were separated on a 3–12% SDS-polyacrylamide gradient gel. Proteins were transferred to a polyvinylidene difluoride (PVDF) membrane (Merck), which was then blocked for 1 h at room temperature in blocking buffer comprising Tris-buffered saline (TBS) containing 5.0% Difco™ skim milk (Becton, Dickinson and Company, Franklin Lakes, NJ, USA) and 0.1% Tween 20.

Next, the PVDF membrane was incubated with the following primary antibodies in blocking buffer overnight at 4°C: goat anti-actin (1:2500, Santa Cruz Biotechnology, TX, USA) or mouse anti-MBP (1:1000, Abcam). The membrane was washed in T-TBS, followed by a 1 h incubation at room temperature with horseradish peroxidase (HRP)-conjugated anti-goat or anti-mouse IgG (Jackson ImmunoResearch, PA, USA) antibodies diluted 1:2500 in T-TBS. The PVDF membrane was then washed in T-TBS. The antigen-antibody peroxidase complex was detected using enhanced chemiluminescence (ECL Select, GE Healthcare Life Sciences, Sweden) according to the manufacturer's instructions, and images were generated using ImageQuant™ (LAS500, GE Healthcare Life-Sciences). The intensity of each band was determined by Image J software and normalized against actin (loading control). Relative density (%) was expressed as the values for the drug-treated groups $\times 100 /$ the value for the vehicle-treated group.

Quantitative analysis by real-time RT-PCR

cDNA was amplified in 20 μ l of a PCR solution containing 10 μ l of Power SYBR® Green PCR Master Mix (Thermo Fisher Scientific) and primers targeting *p75* (sense: 5'-GCT GGG TTA CCA GCC TGA AC-3', antisense: 5'-GCA GTG GAC TCG CTG CAT AG-3'), *Galectin-3* (sense: 5'-GAC ATC GCC TTC CAC TTT AAC C-3', antisense: 5'-GTC TTT CTT CCC TTC CCC AGT T-3'), and *GAPDH* (sense: 5'-GTT ACC AGG GCT GCC TTC TC-3', antisense: 5'-TGA TGA CCA GCT TCC CAT TC-3'). PCR was performed using the StepOnePlus™ System (Thermo Fisher Scientific) under the following cycling conditions: 95°C for 10 min and 60°C for 1 min, followed by 40 cycles of 95°C for 15 sec and 60°C for 1 min. Fluorescence was detected after each extension step. *GAPDH* was used as a normalization control, and relative mRNA levels were calculated using a comparative C_t method and StepOnePlus™ software (Thermo Fisher Scientific).

Preparation and infection of MBP::Venus lentiviral vector (LVV)

In the construct, Venus fluorescent protein (EYFP variant) (19) was expressed under the control of the 0.6 kb Schwann cell enhancer 1 (SCE1; Schwann cell-specific *MBP* enhancer element) (20) and the minimal promoter from the gene encoding rat heat-shock protein 1A (*Hspa1a*) gene. PCR for vector construction was performed with Q5 DNA polymerase (New England Biolabs, MA, USA). For construction of pCSII-rHspa1a miniP-Venus-PRE (rHspa1a::Venus), rat *Hspa1a* minimal promoter was amplified from

rat genomic DNA and ligated into BamHI-digested pCSII-Venus-PRE (a kindly gift from Dr. Miyoshi and Miyawaki [RIKEN, Japan]) via Infusion reaction (Clontech, CA, USA). For construction of pCSII-rSCE1-Hspa1a-Venus-PRE (*MBP::Venus*), rat SCE1 sequence was amplified from rat genomic DNA, digested with AscI/BamHI, and ligated into rHspa1a::Venus digested with AscI/BamHI. Sequences of primers (Hokkaido System Science, Sapporo Japan) were as follows: rat Hspa1a (sense: 5'- CAG CGG CCG CGG ATC CTG ATT GGC CCA TGG GAG GGT GGG CG -3', antisense: 5'- TCA CCA TGG TGG ATC GTC GCC GCT CTC TGC TTC TGG AAG G -3'), AscI SCE1 sense (5'- AAT GGC GCG CCG CAG GCA GCC TGG CAG GCA GCC A -3'), and BamHI SCE1 antisense (5'- GGC GGA TCC GAA CTC TCT AGG CAA GAA GAC CTG T -3'). The constructs were verified by Sanger sequencing (Fasmac, Atsugi, Japan).

MBP::Venus LVV was produced and purified as reported previously (21).

At 1 day after seeding on plates, 60% confluent purified Schwann cells were exposed to *MBP::Venus* LVV diluted 1:7500 in maintenance medium for 24 h. After incubation, medium containing LVV was washed out and replaced with fresh maintenance medium. After 2 days of culture, the medium was replaced with differentiation medium.

von Frey filament test (up-down method)

Male mice received an intraperitoneal (i.p.) injection of paclitaxel (4 mg/kg) or saline on Days 0, 3, 5, and 7 as described previously (22). Mechanical sensitivity was assessed by measuring the paw withdrawal threshold using calibrated von Frey filaments (Touch Test; North Coast Medical, Morgan Hill, CA, USA) as previously described with slight modifications (23,24). On the day of each von Frey test, mice were acclimatized on a metal mesh floor in small Plexiglas cubicles (length, 9 cm; width, 5 cm; height, 5 cm) for 1 h. Mechanical sensitivity was measured using a set of seven calibrated von Frey filaments of increasing strength (0.008, 0.02, 0.04, 0.07, 0.16, 0.4, and 1 g) applied to the plantar surface of the right hind paw until the filament bent slightly for a few seconds. The 0.16 g filament was applied first. Each filament was consecutively applied five times, and a positive or negative response was defined as a paw withdrawal response from pressure of a filament or lack of a response within 6 sec, respectively. The paw withdrawal response was scored as follows: 0, no response; 1, moderate effort to avoid the probe; and 2, vigorous effort to escape the stimulus, such as jumping, shaking, or biting at the right hindpaw. After five applications of each filament, if total score was below 5, the next

higher filament was applied. If the total score was equal to or greater than 5, the next smaller filament was applied. This process was continued until the filaments were changed four times after the first breaking point, and then the 50% paw withdrawal threshold was converted to the cutaneous nociceptive threshold using an adaptation of the Dixon up–down paradigm (24). The measurement of 50% paw withdrawal threshold was performed at 5 days after the previous drug injection. The tests were conducted by the same investigator, who was blinded to the treatment group of each animal.

Immunohistochemical analysis of mouse sciatic nerve sections

On the day after the last injection, mice were deeply anesthetized with pentobarbital (50 mg/kg, i.p.; Nacalai Tesque) and intra-cardially perfused with freshly prepared 4% paraformaldehyde in 0.1 M phosphate buffer (PB). Subsequently, bilateral sciatic nerves were quickly removed. Sciatic nerve sections were post-fixed in 4% paraformaldehyde for 4 h and permeated with 15% sucrose solution in 0.1 M PB for 24 h at 4°C. The sciatic nerve sections were then frozen in an embedding compound (Sakura Fintek USA, CA, USA) and stored at -80°C until use. Frozen longitudinal segments of sciatic nerve were cut with a freezing cryostat (Leica CM 1850, Leica Microsystems, Germany) (16 µm thick) and thaw-mounted on MAS-coated glass slides (Matsunami Glass Ind). The sections were then blocked in blocking buffer (PBS containing 0.1% Tween 20 and 5% normal goat serum, Vector Laboratories) for 1 h at room temperature and then incubated for 24 h at 4°C with the following primary antibodies: mouse anti-p75 (1:500, Abcam) plus rabbit anti-MAP2 (1:250, Merck Millipore) or rat anti-glial fibrillary acidic protein (GFAP, 1:50, Merck Millipore), or rabbit anti-p75 (1:100, Abcam) plus mouse anti-galectin-3 (1:150, Abcam). The antibodies were rinsed away using PBS (three times) and incubated for 1.5 h at room temperature with appropriate secondary antibodies conjugated to Alexa Fluor™ 488 and/or 594 (1:200). The slides were then cover-slipped with Vectashield. All images were acquired under a laser scanning confocal microscope (Fluoview FV10i Confocal Microscope, Olympus Corporation). Nine fields (three fields × three independent samples) were selected randomly per group, and the immunoreactive signal intensity was measured using a computer-assisted system (Image J). Relative intensity (%) was expressed as the value for the drug-treated groups × 100 / the value for the vehicle-treated group.

Statistical analysis

Data were analyzed using GraphPad Prism 5 (GraphPad Software, La Jolla, CA, USA) and expressed as the mean \pm S.E.M. Differences between two groups were compared using Student's t-test. Data from more than two groups were compared using one-way or two-way analyses of variance (ANOVA), followed by the Tukey's multiple comparison test. In all cases, differences of $p < 0.05$ were considered statistically significant.

Results

Paclitaxel induces morphological changes in cultured Schwann cells

I utilized cultured primary Schwann cells from the sciatic nerves of neonatal rats to evaluate the direct effect of anti-cancer agents. After 2 days of culture in differentiation medium, Schwann cells showed a differentiated cell phenotype, characterized by increased expression of the mRNA of MBP, a major myelin protein (Fig. 1-1A). Before cell differentiation, there was little or no expression of MBP. I further confirmed sufficient induction of Schwann cell differentiation by noting almost complete disappearance of mRNA expression of an immature Schwann cell marker, p75 neurotrophin receptor (Fig. 1-1A).

I next evaluated the effects of paclitaxel on the viability of differentiated Schwann cells using a MTT assay. Paclitaxel reduced the viability of Schwann cells in a concentration-dependent manner after 48 h of treatment (Fig. 1-1B). Paclitaxel (10, 30 and 100 nM) showed significant cytotoxic effects against Schwann cells after 48 h. Ten nM was taken to be the minimum concentration showing a significant effect against Schwann cells.

To gain further insight into the direct effects of anti-cancer agents on Schwann cells, I examined the effects of paclitaxel on the morphology of differentiated Schwann cells (Fig. 1-1C). Differentiated cells had a typical Schwann cell phenotype, being bipolar and spindle shaped, with a small cytoplasm. Cells also stained positive for MBP. Treatment with paclitaxel (10 nM) for 48 h reduced the number of MBP-positive Schwann cells. Expression of MBP was significantly lower after treatment with paclitaxel (1 and 10 nM) in a concentration-dependent manner (Fig. 1-1D). Paclitaxel caused marked morphological changes, characterized by retraction of bipolar processes and a rounded shape (Fig. 1-1C).

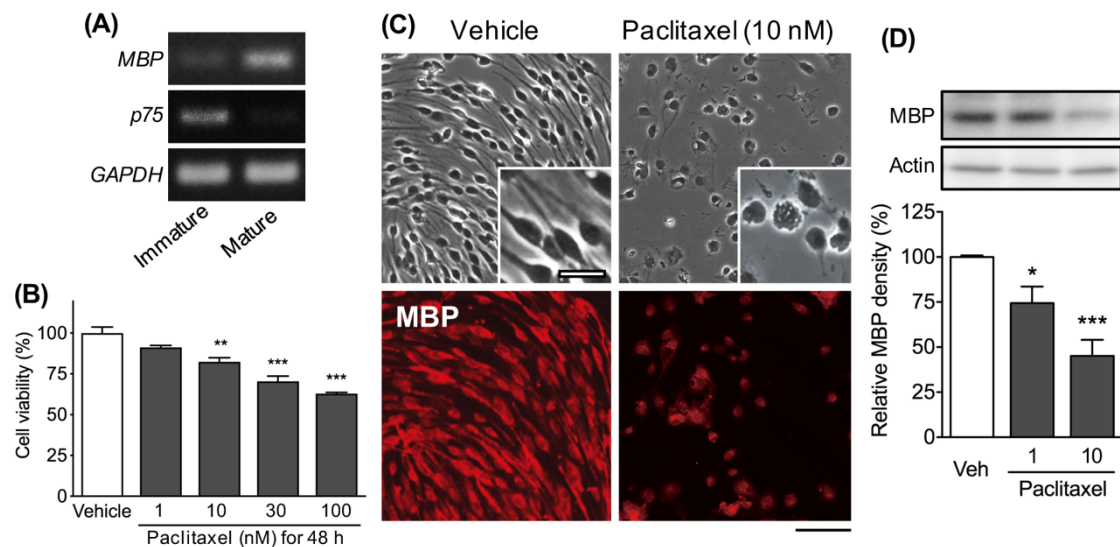


Fig. 1-1. Effects of paclitaxel on Schwann cell morphology and MBP expression. (A) Representative RT-PCR showing expression of MBP and p75 mRNAs in Schwann cells just before (left lane) and 2 days after (right lane) differentiation. GAPDH is shown as an internal control. (B) Viability of Schwann cells 48 h after exposure to vehicle (0.1% DMSO) or paclitaxel (1, 10, 30 or 100 nM). *n* = 3–5. (C) Phase (upper) and fluorescence (lower) micrographs of differentiated Schwann cells labeled with an anti-MBP antibody. Differentiated Schwann cells were treated with vehicle (0.1% DMSO) or paclitaxel (10 nM) for 48 h. Scale bar: 100 μ m (25 μ m in enlarged images). (D) Expression of MBP in Schwann cells 48 h after treatment with vehicle (Veh, 0.1% DMSO), paclitaxel (1 and 10 nM) was analyzed by Western blotting. (Upper panels) Representative Western blot showing expression of MBP and actin. (Lower panels) Quantification of band intensity. The intensity of each band was normalized to that of actin (loading control). *n* = 5–8. Data are expressed relative to the value in vehicle-treated cells (% of control) and are represented as means \pm S.E.M. **p* < 0.05, ***p* < 0.01 and ****p* < 0.001.

Paclitaxel induces impairment of myelin formation in a mixed culture of Schwann cells and DRG neurons

The direct effect of paclitaxel on the viability and morphology of rat primary DRG neurons were also investigated (Fig. 1-2A). Primary DRG neurons stained with an antibody specific for the neuronal marker MAP2 were spherical, with multi-neuritic processes. Treatment with paclitaxel (10 nM) for 48 h did not affect the viability or morphology of primary DRG neurons. By contrast, exposure to paclitaxel at higher concentrations (100 nM) reduced the number of neurons and their dendritic trees, and shortened the length of the neuritic processes, when compared with vehicle treatment.

The next study was undertaken to determine whether treating Schwann cell/DRG neuron co-cultures with paclitaxel leads to demyelination. In a mixed culture of Schwann cells and DRG neurons, Schwann cells differentiated along the DRG axons and eventually formed MBP-positive myelin segments, as indicated by the apparent overlap

of MAP2- and MBP-immunoreactivities (IRs) (Fig. 1-2B). Treatment with paclitaxel (10 nM) for 48 h led to a marked reduction in MBP-IR, suggesting loss of myelinating Schwann cells in the co-cultures (Fig. 1-2C). However, the treatment did not affect MAP2-positive neural axons.

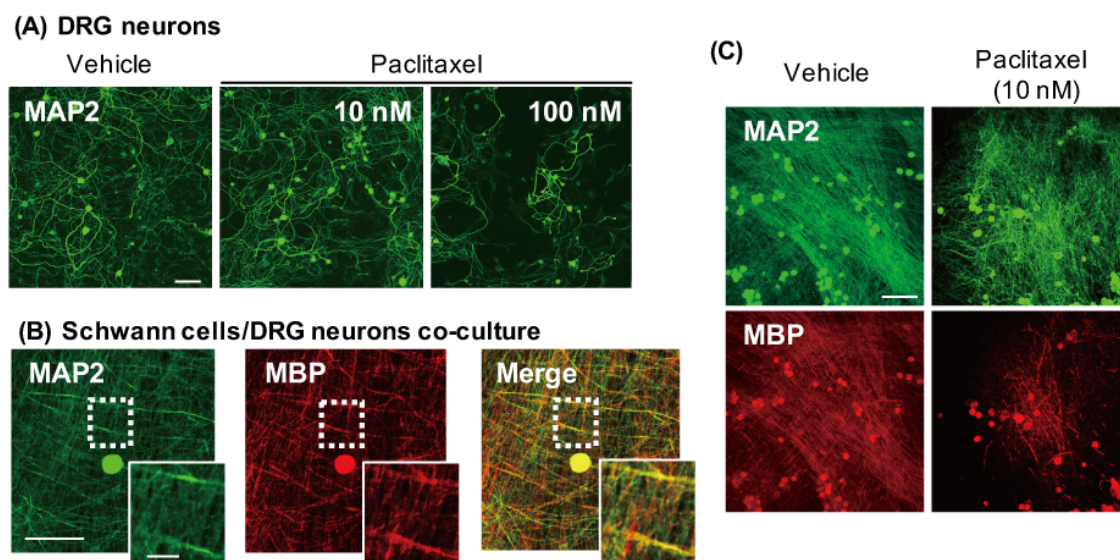


Fig. 1-2. Effects of paclitaxel on primary cultured DRG neurons or co-cultures of Schwann cells and DRG neurons. (A) Immunofluorescence staining of primary cultured DRG neurons for MAP2. Primary cultured DRG neurons were treated with vehicle (0.1% DMSO) or paclitaxel (10 and 100 nM) for 48 h. Scale bar: 100 μ m. (B) In vitro myelination was induced in a co-culture of DRG neurons and Schwann cells. Representative images of cultures immunostained for MAP2 (green) and MBP (red) are shown. Scale bar: 100 μ m (25 μ m in enlarged images). (C) Co-cultures were treated with vehicle (0.1% DMSO) or paclitaxel (10 nM) for 48 h. Scale bar: 200 μ m.

Taxanes induce upregulation of p75 and galectin-3 in cultured Schwann cells

To better understand the direct effect of paclitaxel on Schwann cells, I focused on the expression pattern of p75 and galectin-3, markers of immature and dedifferentiated Schwann cells, respectively. The expression levels of *p75* and *Galectin-3* mRNAs were significantly higher in the paclitaxel-treated group than in the vehicle-treated group (Fig. 1-3A, B). Like paclitaxel, treatment with docetaxel (10 nM), another taxane agent, induced an increase in p75- and galectin-3-IRs in Schwann cells (Fig. 1-3C), in addition to a decrease in cell viability and morphological changes.

To verify that galectin-3 upregulation following taxane treatment was specific for p75-positive dedifferentiated Schwann cells, rather than p75-positive immature Schwann cells mixed in heterogeneous cell populations, I visualize mature Schwann cells by transducing cultured Schwann cells with a LVV encoding the *MBP::Venus* reporter (Fig. 1-4A). This culture system allows me to distinguish between dedifferentiated Schwann cells

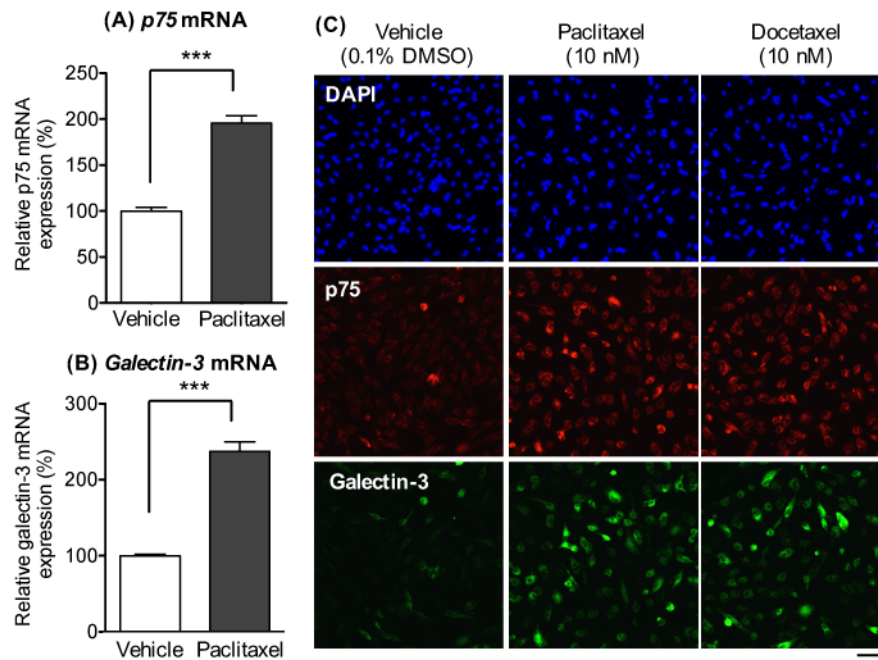


Fig. 1-3. Effects of taxanes on expression of p75 and galectin-3 in primary cultured Schwann cells. Schwann cells were treated with vehicle (0.1% DMSO), paclitaxel (10 nM) or docetaxel (10 nM) for 48 h. **(A, B)** Quantitative real-time RT-PCR analysis of *p75* (A) and *Galectin-3* (B) mRNA expression in Schwann cells. Each column represents the mean \pm S.E.M. $n = 3$. $***p < 0.001$. **(C)** Immunofluorescent staining for DAPI (blue), p75 (red) and galectin-3 (green). Scale bars: 50 μ m.

transitioned from Venus-positive mature Schwann cells upon paclitaxel treatment (i.e., Venus/p75-double positive cells) and immature Schwann cells (i.e., Venus-negative/p75-positive cells) in mixed cell populations. Before cell differentiation, Schwann cells exhibited a considerable p75-IR, but only weak MBP-IR and Venus fluorescence (Fig. 1-4B). After 2 days of culture in differentiation medium, Schwann cells exhibited a differentiated phenotype, characterized by increased MBP-IR and disappearance of p75-IR (Fig. 1-4B). In these differentiated Schwann cells, Venus fluorescence was elevated and highly co-localized with MBP-IR. However, exposure of differentiated Schwann cells to paclitaxel (10 nM) for 48 h decreased MBP-IR (Fig. 1-4C) and increased both p75- and galectin-3-IRs relative to Schwann cells treated with vehicle alone (0.1% DMSO) (Fig. 1-4D). The increased p75- and galectin-3-IRs co-localized with Venus fluorescence in paclitaxel-treated Schwann cells (Fig. 1-4D). These findings highlight the upregulation of galectin-3 in dedifferentiated Schwann cells derived from Venus-expressing mature Schwann cells, as illustrated in Fig. 1-4E.

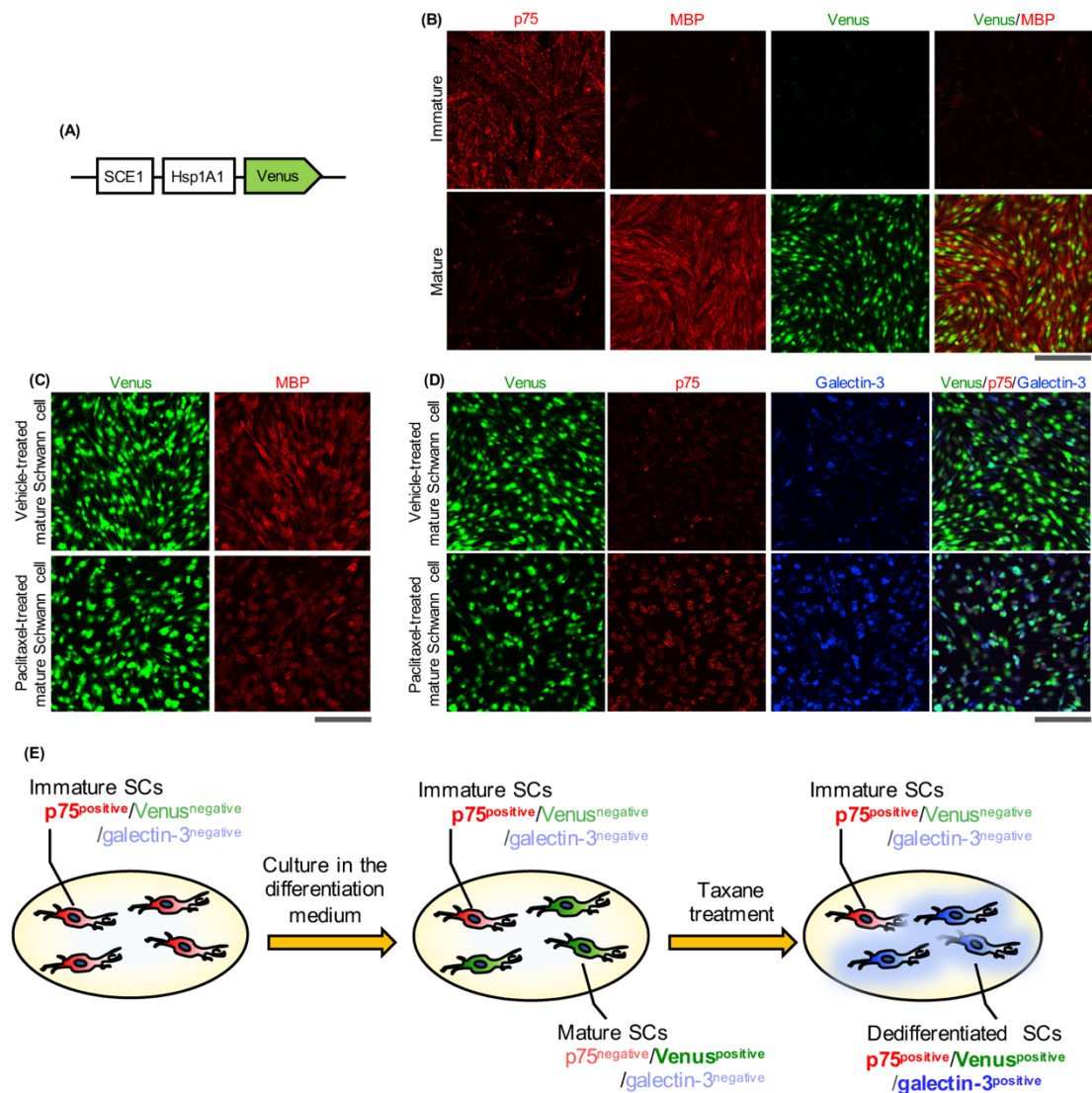


Fig. 1-4. Galectin-3 increases in dedifferentiated Schwann cell culture upon taxane treatment. (A) Illustration of MBP::Venus LVV construct. LVV was constructed by insertion of the minimal promoter from the gene encoding rat *Hspa1a* followed by the *Venus* gene downstream of the 0.6 kb SCE1. (B) Fluorescence micrographs of Schwann cells transfected with MBP::Venus LVV before (immature, *upper panels*) or after differentiation (mature, *lower panels*). Immature primary rat Schwann cells were exposed to MBP::Venus LVV for 24 h, and the culture medium was replaced with differentiation medium. The fixed cells were immunolabeled for p75 (red) or MBP (red). (C, D) Representative confocal micrographs showing Venus fluorescence (green) and MBP (C; red) or p75 (D; red)/galectin-3 (D; blue)-IR in primary cultures of rat Schwann cells. Venus-expressing mature Schwann cells were treated with vehicle (0.1% DMSO) or paclitaxel (10 nM) for 48 h. Scale bars: 100 μ m. (E) Schematic summarizing the results in Fig. 1-4. After 2 days of culture in differentiation medium, p75-positive/Venus-negative immature Schwann cells (SCs, shown in red) differentiated into p75-negative/Venus-positive mature SCs (shown in green). Taxane treatment induced conversion of mature SCs into p75/Venus-double positive dedifferentiated SCs (shown in blue). Elevated expression of galectin-3 was detected in these dedifferentiated SCs, but not in immature SCs, after taxane treatment.

Paclitaxel causes Schwann cell dedifferentiation in the mouse sciatic nerves

When mice were repeatedly treated with paclitaxel (4 mg/kg × 4, i.p.), the 50% paw withdrawal threshold in response to tactile stimuli decreased gradually at 4 and 7 days after the first injection (Fig. 1-5A). Under these conditions, p75-IR in sciatic nerves of mice treated with paclitaxel was also examined (Fig. 1-5B). Repeated injection of paclitaxel increased p75-IR in the longitudinal section of the sciatic nerve, although only weak p75-IR was detected in the same section from saline-treated mice. The p75-immunolabeling pattern appeared to surround MAP2-positive neural axons, and was localized in GFAP-positive Schwann cells. Consistent with this, galectin-3-IR in longitudinal sections of sciatic nerve from paclitaxel-treated mice also increased. Galectin-3-IR in the sciatic nerve of paclitaxel-treated mice was highly co-localized in

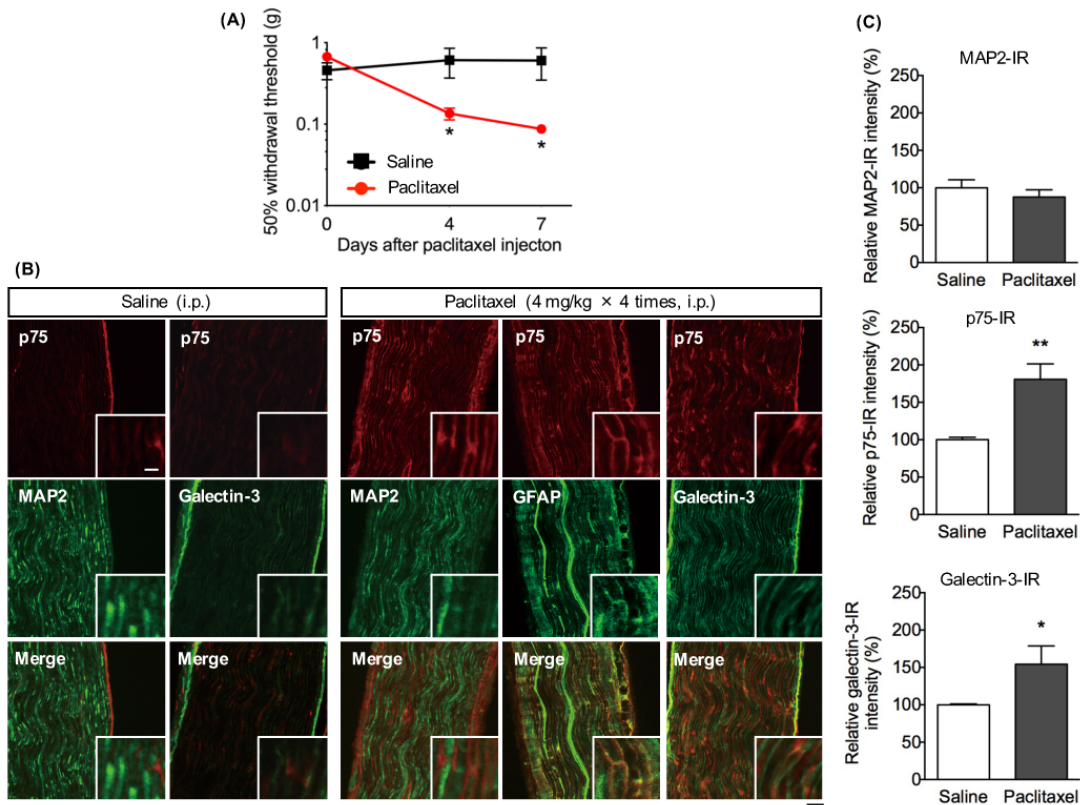


Fig. 1-5. Changes in the expression of p75 and galectin-3 in sciatic nerves obtained from mice treated with paclitaxel. Paclitaxel (4 mg/kg, i.p.) was injected on Days 0, 3, 5, and 7. At 1 day after the last injection, mice were fixed and subjected to immunohistochemical assay. **(A)** Changes in paw withdrawal threshold in response to mechanical stimuli in the right hindpaw. Each point represents the mean ± S.E.M. $n = 4-8$. * $p < 0.05$ and ** $p < 0.01$ vs. the vehicle-treated group. **(B)** Longitudinal sections of sciatic nerve isolated from saline- or paclitaxel-treated mice were co-immunolabeled for p75 (red), or MAP2, GFAP or galectin-3 (green). Scale bar: 50 μm (10 μm in enlarged images). **(C)** Quantification of the intensity of fluorescence associated with MAP2, p75 or galectin-3. Each column represents the mean ± S.E.M. $n = 3-5$. * $p < 0.05$ and ** $p < 0.01$ vs. the vehicle-treated group.

GFAP-positive Schwann cells, whereas only weak galectin-3-IR was detected in the sciatic nerve of saline-treated mice. Quantitative analysis revealed that p75- and galectin-3-IRs in the sciatic nerve of paclitaxel-treated mice was significantly higher than that in saline-treated mice, whereas, there was no difference in MAP2-IR between paclitaxel- and saline-treated mice (Fig. 1-5C).

Discussion

Here, I showed for the first time that taxanes induce dedifferentiation of myelin-forming Schwann cells with their morphological changes at a lower concentration than that required to induce neurotoxicity.

Schwann cell precursors, which represent the first transitional stage of the Schwann cell lineage, differentiate into immature Schwann cells, which then give rise to promyelinating Schwann cells. These cells eventually develop into mature myelin-forming Schwann cells (25). Schwann cells express specific lineage markers at each stage of differentiation (26). Consistent with previous studies (15,26), I found that Schwann cells dissociated from the sciatic nerve showed an immature phenotype, with low expression of a myelin-associated molecule (MBP) and high expression of p75. I also observed accelerated transformation of Schwann cells into differentiated Schwann cells when cultured in differentiation medium, characterized by almost complete disappearance of p75 expression and increased expression of MBP (27,28). I showed that *in vitro* treatment with paclitaxel at clinically relevant plasma concentrations (29) decreased Schwann cell viability and caused dynamic morphological changes in Schwann cells at a relatively lower concentration (10 nM).

It should be noted that the treatment with a relatively low concentration of paclitaxel reduced myelin-forming Schwann cells in the Schwann cell/DRG neuron co-cultures without causing damages to the neurons. Furthermore, repeated treatment with paclitaxel had no significant effect on the MAP2-positive axons of sciatic nerves from mice with mechanical allodynia. Thus, the present findings provide evidence that Schwann cells might be a candidate target of taxanes that induce CIPN. A reduction of myelin-forming Schwann cells causes neurological dysfunction or abnormal neural conduction, both of which may underlie the pathogenesis of diabetic neuropathy (30) and Charcot-Marie-Tooth disease (31). Thus, taxane-induced impairment of myelin-forming Schwann cells

with dynamic morphological changes seems to result in the myelin instability and reduction in myelin sheath integrity. Analysis of nerve action potential recordings in rodents suggested that multiple injection of paclitaxel reduces the peak amplitude and conductance velocity (32,33). In addition, the reduction of the peak amplitude is observed in humans treated with paclitaxel (34). It is possible that functional impairment of peripheral neurons may be due to myelin instability and a reduction of myelin sheath integrity induced by taxanes.

The results presented herein show that a lower concentration of paclitaxel directly affects Schwann cells, although I never clarified its temporal and functional effects on DRG neurons. Thus, my present data do not exclude the possibility that preferential impairment of peripheral neurons by the taxanes is responsible for CIPN. Nevertheless, the present data suggest that the direct effects of taxanes on Schwann cells might contribute to the pathogenesis of CIPN in conjunction with their direct impairment of peripheral neurons.

The key finding of this study is that treatment with taxanes causes dedifferentiation of Schwann cells, as indicated by increased expression of an immature Schwann cell marker, p75, and a dedifferentiated Schwann cell marker, galectin-3, and reduced expression of a differentiated Schwann cell marker, MBP. However, primary cultures of mature Schwann cells were composed of a heterogeneous population consisting of a large number of differentiated cells and a few immature cells. Using the *MBP::Venus* expression system dependent on Schwann cell maturation, I found that paclitaxel increased galectin-3 expression in p75-positive dedifferentiated Schwann cells derived from mature Schwann cells, rather than p75-positive immature Schwann cells already present in the heterogeneous population. I also showed increased expression of p75 and galectin-3 in Schwann cells surrounding the neural axon in sciatic nerves isolated from mice with paclitaxel-induced mechanical hypersensitivity. Myelinating Schwann cells can transform into an immature phenotype and re-enter the cell cycle to support nerve regeneration in response to peripheral nerve injury (35). p75 is induced in demyelinating Schwann cells during Wallerian degeneration and regrowth of peripheral axons, and is involved in Schwann cell dedifferentiation (36,37). Dedifferentiated Schwann cells also show high expression of galectin-3, which is not detectable in immature Schwann cells and plays an important role in lectin-mediated phagocytosis of degraded material at the site of injury (17,38). Thus, to the best of my knowledge, the present data are the first to

suggest that taxanes induce Schwann cells to dedifferentiate into an immature state, which is akin to Schwann cell transformation after the nerve injury. Recently, Nobusue *et al.* proposed a new mechanism to explain the relationship between cytoskeletal dynamics and cellular differentiation of adipocytes (39). They suggest that depolymerization of actin fibers in adipocytes triggers the differentiation program, which is mediated by increased expression of a transcriptional regulator of adipogenesis. Of particular note is that, taxanes, which prevents microtubule depolymerization, facilitated transformation of Schwann cells into an immature state, characterized by increased expression of p75 and galectin-3. These results support the idea that taxane-mediated inhibition of cytoskeletal dynamics may induce dedifferentiation of Schwann cells, although further studies are needed to identify the underlying molecular mechanisms. The present findings allow us to consider that a unique phenomenon, taxane-induced dedifferentiation of Schwann cells, is likely responsible for the disruption of cross talk between myelin-forming Schwann cells and axons, resulting in induction of CIPN after taxane treatment.

In conclusion, the data presented herein suggest that taxanes cause dedifferentiation of Schwann cells. The phenomena may disrupt cross talk between myelin-forming mature Schwann cells and axons, thereby promoting peripheral neuropathy induced by taxanes.

Chapter 2: Schwann cell-derived galectin-3 has pro-nociceptive roles in taxane-induced peripheral neuropathy

Introduction

Galectin-3, the β -galactoside binding protein, is localized in the cytoplasm, nucleus, and plasma membrane, and can be secreted into the extracellular compartment, where it serves as an immune cell chemoattractant (40). A number of earlier clinical studies showed that galectin-3 derived from cardiac fibroblasts are increased in plasma of heart failure patients with reduced ejection fraction (41-43). In addition, extracellular galectin-3 leads to microglial activation in the brain via Toll-like receptors or triggering receptor expressed on myeloid cells 2 (TREM2) signaling, thereby eliciting neuroinflammation associated with the progression of Alzheimer's disease (44). On the other hand, during Wallerian degeneration after peripheral nerve injury (38), dedifferentiated Schwann cells show high expression of galectin-3, which plays an important role in lectin-mediated phagocytosis of degraded material at the site of injury. In Chapter 1, I found that galectin-3 is upregulated in primary cultures of rat Schwann cells following paclitaxel treatment and Schwann cells in the sciatic nerve of paclitaxel-related CIPN model mice. However, the role of galectin-3 upregulated in Schwann cells in CIPN pathogenesis is still unknown. Reports of pathogenic roles for extracellular galectin-3 in some diseases have raised the intriguing hypothesis that Schwann cell-derived galectin-3 is also released into the extracellular compartment (i.e., the blood circulation) and participates in the pathogenesis of taxane-related CIPN.

In this chapter, I found that the plasma galectin-3 level was elevated in both taxane-treated breast cancer patients accompanying CIPN and a mouse model of taxane-related CIPN. I then showed that plasma galectin-3 originates from Schwann cells within the peripheral nerves. Furthermore, I demonstrated for the first time that Schwann cell-derived galectin-3 plays a critical role via macrophage infiltration in the development of taxane-induced peripheral neuropathy.

Materials and Methods

Measurement of human plasma galectin-3

A self-controlled, prospective observational study was conducted. The clinical trial was approved by the Ethics Committee of Kyoto University Graduate School and Faculty of Medicine (G424) in accordance with Helsinki guidelines and registered with the University Hospital Medical Information Network. All subjects provided written informed consent. Patients with a history of heart failure or peripheral sensory/motor diseases (e.g., diabetes or Carpal tunnel syndrome) that could induce peripheral neuropathy, or who were expected to receive certain drugs (e.g., platinum anti-cancer agents) during the test period that could induce peripheral neuropathy, were excluded. Plasma galectin-3 level was determined using a commercially available ELISA kit (Human Galectin-3 Platinum ELISA, BMS279/4, Thermo Fisher Scientific).

Animals

All animal experiments were approved and performed as described in Chapter 1. Pregnant Wistar/ST rats, male C57BL/6J JmsSlc (5–7 weeks) and C57BL/6-Tg(CAG-EGFP) C14-Y01-FM131Osb transgenic mice (male C57BL/6GFP transgenic mice) were obtained from Japan SLC. C57BL/6.Cg-*Lgals3^{tm1Poi}*/J transgenic (*Galectin-3^{-/-}*) mice were obtained from Jackson Laboratory (ME, USA) via Charles River Laboratories Japan (Kanagawa, Japan). Male *Galectin-3^{-/-}* mice (6–14 weeks) were used for experiments.

Reagents

For *in vivo* experiments, paclitaxel 30 mg/5mL (Nippon Kayaku, Tokyo, Japan) was diluted with saline (2 mg/mL). Because approximately 16.7% ethanol was present in the dilute solution of paclitaxel, saline containing ethanol at the same concentration was used as the vehicle control. Docetaxel 20 mg/mL (Nippon Chemiphar, Tokyo, Japan) containing about 50% ethanol was diluted with saline (2 mg/mL). 5% Ethanol diluted in saline was used as the vehicle control for docetaxel. A systemic macrophage-depleting agent, clodronate liposomes (Clophosome-N; FormuMax Scientific, CA, USA), and its control liposomes (FormuMax Scientific) were used without dilution. The galectin-3 inhibitor TD-139 (ChemScene LLC, NJ, USA) was dissolved in DMSO at 100 mM. The stock solution was diluted in saline to 15 mg/kg immediately prior to injection, and saline containing 2.3% DMSO was used as vehicle.

For *in vitro* experiments, stock solutions of paclitaxel and docetaxel were prepared as described in Chapter 1. The nuclear factor- κ B (NF- κ B) inhibitor SC75741 (Selleck Chemicals, TX, USA) was prepared in DMSO at concentrations of 10 mM.

Recombinant mouse galectin-3 (rGalectin-3; >95% pure; R&D Systems, MN, USA, #9039-GA) was dissolved in PBS at a concentration of 10 nM or diluted in the appropriate culture medium at a concentration of 2 pM prior to use for *in vivo* and *in vitro* assays, respectively. PBS was used as the vehicle for rGalectin-3.

Mouse model of taxane-induced CIPN

Mice were i.p. injected with paclitaxel (20 mg/kg), or docetaxel (20 mg/kg), or its vehicle (16.7% or 5% ethanol, respectively) twice a week (paclitaxel; on days 1 and 2, docetaxel; on days 1 and 3) for a total of 1–8 weeks.

von Frey filament test (scored method)

Mice were habituated as described in Chapter 1. Mechanical sensitivity was evaluated using a calibrated 0.16 g von Frey filament. The paw withdrawal response was scored as follows: 0, no response; 1, moderate effort to avoid the probe; and 2, vigorous effort to escape the stimulus. Each trial contained five applications of the von Frey filament, each of which was scored as 0, 1, or 2. After five applications, the total response score was calculated.

Measurement of galectin-3 level in mouse plasma or culture supernatant of Schwann cells

Galectin-3 concentration in mouse plasma or culture supernatant of rat primary Schwann cells was determined using the Mouse LGALS3/Galectin-3 ELISA Kit (#LS-F494, LifeSpan BioSciences, Seattle, WA, USA) or Rat LGALS3/Galectin-3 ELISA Kit (#LS-F3877, LifeSpan BioSciences), respectively. Mouse blood was collected into tubes (Becton, Dickinson and Company, NJ, USA) containing EDTA. Blood was centrifuged at $800 \times g$ for 15 min at 4°C, and plasma samples were obtained. Schwann cell supernatant was collected 48 h after exposure to each anti-cancer agent. All samples were frozen at -80°C until analyses.

Quantitative analysis by real-time RT-PCR

PCR was performed as described in Chapter 1. Details of synthesized primers are described in Table 2-1.

Knockdown of NF- κ B p65 in Schwann cells

After the incubation in the differentiation medium for 24 h, Schwann cells were transfected with NF- κ B p65 (NM_199267.2) siRNA (designed and synthesized by NIPPON GENE, Tokyo, Japan) or universal negative control siRNA using Lipofectamine RNAiMAX (Thermo Fisher Scientific) for 24 h. Twenty-four h after the washout of siRNA, Schwann cells were treated with vehicle (0.1% DMSO), paclitaxel (10 nM) or docetaxel (10 nM) for 48 h.

Immunocytochemistry, Immunohistochemistry and Western blotting

The experiments were performed as described in Chapter 1.

The following primary antibodies were used for immunocytochemistry: rat anti-MBP (1:300, Merck, #MAB386), mouse anti-p75 (1:1000, Merck, #MAB365), rabbit anti-p75 (1:500, Abcam, #ab38335), or mouse anti-galectin-3 (1:200, Abcam, #ab2785).

For immunohistochemistry, mouse anti-galectin-3 (1:166), rat anti-GFAP (1:50, Merck, #345860), rabbit anti-ionized calcium binding adapter molecule 1 (Iba1; 1:500, Wako Pure Chemical Industries, #019-19741), rat anti-CD31 (1:100, Becton, Dickinson and Company, #550274), or rat anti-inducible nitric oxide synthase (iNOS; 1:20, Thermo Fisher Scientific, #14-5920-82) was used. For iNOS staining, Tyramide Signal Amplification system (Akoya Biosciences, CA, USA) was used. Relative galectin-3-IR (%) is expressed as $100 \times (\text{value for paclitaxel-injected group}) / (\text{value for vehicle-treated group})$. Iba1, GFP or iNOS-immunolabeled cells in each section were visually counted. The area of the parenchyma of sciatic nerve was measured using ImageJ. From these two values, the average number of Iba1, GFP or iNOS-positive cells per mm^2 was calculated.

For immunoblot detection, the PVDF membrane was incubated with mouse anti-galectin-3 (1:1000), rabbit anti-NF- κ B p65 (1:1000, Cell Signaling Technology, MA, USA, #8242), rabbit anti-phospho NF- κ B p65 (Ser536) (1:1000, Cell Signaling Technology, #3033) or mouse anti- β -actin (1:20000, SIGMA-ALDRICH, #A1978).

Migration Assay of RAW 264.7 cells

The murine macrophage cell line RAW 264.7 (TIB-71) was purchased from ATCC (VA, USA). Migration was monitored using the CytoSelect 96-Well Cell Migration Assay (8 μ m, Fluorometric Format; Cell Biolabs, San Diego, CA, USA) as described previously (45).

Focal application of galectin-3 to the mouse sciatic nerve

Surgery was performed as previously reported (45) with minor modifications. Mice were anesthetized with pentobarbital (50 mg/kg, i.p.), and then the right sciatic nerve was exposed in the popliteal fossa without damaging the perineurium. The right sciatic nerve 2–3 mm proximal to the trifurcation was loosely enwrapped with gauze containing vehicle (PBS) or 10 nM rGalectin-3 without inducing any nerve injury.

Generation of GFP-bone marrow (BM) chimeric mice and Flow cytometry assay

BM transplantation and Flow cytometry to determine the purity of GFP-positive cells in peripheral blood after BM transplantation was conducted as previously reported (45,46).

Statistics

Data were analyzed using GraphPad Prism 8 (GraphPad Software) and expressed as means \pm S.E.M. Differences between two groups were compared with the unpaired *t*-test or Mann–Whitney U-test. Data from more than two groups were compared by one-way or two-way ANOVA, followed by Bonferroni's *post hoc* comparison test. In all cases, *p* < 0.05 was considered statistically significant.

Other experiments were performed as described in Chapter 1.

Table 2-1. Sequences of synthesized primers used in real-time RT-PCR

Target name	Species		Primer sequence	GenBank™ sequence accession number
<i>Galectin-3</i>	Mouse	Sense	5'-TCA GCC TTC CCC TTT GAG AG-3'	BC138790.1
		Antisense	5'-AGC GCT GGT GAG GGT TAT GT-3'	
	Rat	Sense	5'-GAC ATC GCC TTC CAC TTT AAC C-3'	NM_031832.1
		Antisense	5'-GTC TTT CTT CCC TTC CCC AGT T-3'	
<i>Nf-κb p65</i>	Rat	Sense	5'-GCG CAT CCA GAC CAA CAA TA-3'	NM_199267
		Antisense	5'-AAA AAT CGG ATG CGA GAG GA-3'	
<i>Cd86</i>	Mouse	Sense	5'-CTT TCA TTC CCG GAT GGT GT-3'	NM_019388.3
		Antisense	5'-GAG CAG CAT CAC AAG GAG GA -3'	
<i>iNos</i>	Mouse	Sense	5'-CCT GCT TTG TGC GAA GTG TC-3'	NM_001313921.1
		Antisense	5'-CCT CCT TTG AGC CCT TTG TG-3'	
<i>Irf5</i>	Mouse	Sense	5'-CCT TTG CCA TGA ACC ACT CA -3'	NM_001252382.1
		Antisense	5'-GAT GGT GTT GTC CCC ATC CT-3'	
<i>Il-1β</i>	Mouse	Sense	5'-GAC GGA CCC CAA AAG ATG AA-3'	NM_008361.4
		Antisense	5'-GCC TGC CTG AAG CTC TTG TT-3'	
<i>Tnfa</i>	Mouse	Sense	5'-CAA ATG GCC TCC CTC TCA TC-3'	NM_013693.3
		Antisense	5'-CTC CAG CTG CTC CTC CAC TT-3'	
<i>Cd206</i>	Mouse	Sense	5'-GTT GGG GTC AGG CTT CTC TG-3'	NM_008625.2
		Antisense	5'-ACC AAA GCC ACT TCC CTT CA-3'	
<i>Irf4</i>	Mouse	Sense	5'-ATC GGC CCA ACA AGC TAG AA-3'	NM_013674.2
		Antisense	5'-TGG CTA GCA GAG GTT CCA CA-3'	
<i>Il10</i>	Mouse	Sense	5'-AAC TGC ACC CAC TTC CCA GT-3'	NM_010548.2
		Antisense	5'-AGG CTT GGC AAC CCA AGT AA-3'	
<i>p75</i>	Rat	Sense	5'-GCT GGG TTA CCA GCC TGA AC-3'	NM_012610
		Antisense	5'-GCA GTG GAC TCG CTG CAT AG-3'	
<i>GAPDH</i>	Mouse	Sense	5'-GCG AGA CCC CAC TAA CAT CA-3'	GU214026.1
		Antisense	5'-TGG TTC ACA CCC ATC ACA AA-3'	
	Rat	Sense	5'-GTT ACC AGG GCT GCC TTC TC-3'	NM_017008
		Antisense	5'-TGA TGA CCA GCT TCC CAT TC-3'	

Results

Plasma galectin-3 level is elevated in taxane-treated breast cancer patients accompanying CIPN

The clinical characteristics of eight female breast cancer patients (mean age [range]: 51.1 [37–79]) and the regimens of taxane-based chemotherapy over 12 weeks are summarized in Tables 2-2 and 2-3, respectively. Because the drugs used concomitantly with taxane-based chemotherapy (i.e., bevacizumab, trastuzumab, pertuzumab, cyclophosphamide, and doxorubicin) are not considered risk factors for CIPN (47-50), I considered it unlikely that they contributed to changes in the plasma galectin-3 levels (Table 2-3).

In plasma samples obtained from eight female breast cancer patients, I checked changes in the galectin-3 concentration before chemotherapy (Baseline), 6 weeks after the initiation of each regimen (6 weeks), and just before the final taxane administration

Table 2-2. Patient characteristics (*n* = 8)

Characteristic	
Mean age (SD), y	51.1 (12.7)
Mean weight (SD), kg	58.4 (8.67)
Mean body mass index (SD), kg/m ²	1.54 (0.137)
Breast cancer, No. (%)	
Left	4 (50)
Right	4 (50)
Left and right	0 (0)
Recurrent	3 (37.5)
Metastasis, No. (%)	1 (12.5)
Treatment, No. (%)	
Neo-adjuvant	1 (12.5)
Adjuvant	7 (87.5)
Taxanes, No. (%)	
Paclitaxel	4 (50)
Docetaxel	4 (50)
Smoker, No. (%)	2 (25)
Administration history of anti-cancer agents with risk of CIPN, No. (%)	
Paclitaxel	0 (0)
Docetaxel	2 (25)
Others	0 (0)

Table 2-3. Chemotherapy regimens and cumulative doses

Patient no.	Anti-cancer agents	Dose (/day)	Administration timing	Cumulative dose of taxane (mg/m ²)
1	Paclitaxel	80 mg/m ²	weekly × 12 cycles	960
2	Paclitaxel	80 mg/m ²	weekly × 12 cycles	960
3	Paclitaxel	90 mg/m ²	on day 1, 8 and 15 of every 4 weeks × 4 cycles	1080
	Bevacizumab	10 mg/kg	on day 1 and 15 of every 4 weeks × 4 cycles	-
4	Paclitaxel	80 mg/m ²	weekly × 12 cycles	960
	Trastuzumab	8 mg/kg (loading dose) followed by 6 mg/kg	on day 1 (loading dose) and every 3 weeks × 4 cycles	-
		Pertuzumab		840 mg/kg (loading dose) followed by 420 mg/kg
Docetaxel	75 mg/m ²	every 3 weeks × 4 cycles		300
5	Cyclophosphamide	600 mg/m ²	× 4 cycles	-
	Docetaxel	75 mg/m ²	every 3 weeks × 4 cycles	300
6	Cyclophosphamide	600 mg/m ²	× 4 cycles	-
	Docetaxel	75 mg/m ²	every 3 weeks × 4 cycles	300
7	Cyclophosphamide	600 mg/m ²	× 4 cycles	-
	Docetaxel	75 mg/m ²	every 3 weeks × 4 cycles	450
8	Cyclophosphamide	500 mg/m ²	× 4 cycles	-
	Doxorubicin	50 mg/m ²		-

Table 2-4. Mean plasma galectin-3 concentration in taxane-treated patients

Galectin-3 concentration	Baseline	6 weeks	12 weeks
(ng/mL; mean ± SD)	5.51 ± 1.70	7.84 ± 4.18	6.88 ± 2.73

(12 weeks) (Fig. 2-1A). CIPN occurred in three of four patients who received 12 weeks of paclitaxel- (Patients No. 2–4) or docetaxel-based chemotherapy (Patients No. 5, 6, and 8) (indicated by filled circles in Fig. 2-1A and B). The average concentration of plasma galectin-3 among these eight patients increased at 6 weeks, and then slightly decreased at 12 weeks after the beginning of chemotherapy (Table 2-4). In patients with CIPN who received therapy of paclitaxel plus bevacizumab (Patient No. 3), paclitaxel/pertuzumab/trastuzumab (Patient No. 4), docetaxel plus cyclophosphamide (TC, Patient No. 5 and 6), and docetaxel combined with cyclophosphamide/doxorubicin (Patient No. 8), the plasma galectin-3 levels were higher than the corresponding baselines. During the study period, the galectin-3 levels did not change in patients

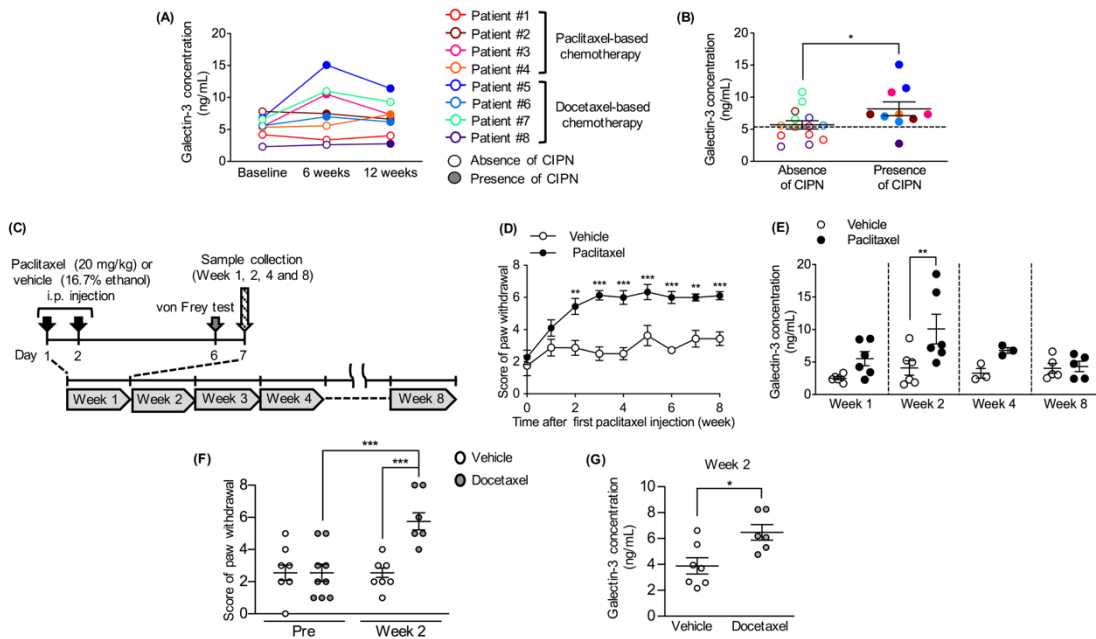


Fig. 2-1. Plasma galectin-3 levels increase in both patients and mice with taxane-related CIPN.

(A) Time-course changes in plasma galectin-3 levels in eight breast cancer patients who underwent paclitaxel- or docetaxel-based chemotherapy. Plasma was collected before the start of chemotherapy (Baseline), at 6 weeks after the initiation of taxane treatment (6 weeks), and just before the final administration of taxanes (12 weeks). Open and filled circles indicate the absence or presence of CIPN, respectively. (B) Comparison of the plasma galectin-3 concentration in the absence or presence of CIPN in the patients shown in (A). Twenty-four measurements of plasma galectin-3 (eight patients \times three time points) were divided into two groups according to the absence ($n = 14$) or presence ($n = 10$) of CIPN. Dashed line indicates mean plasma galectin-3 concentration among seven subjects without cancer. Data are represented as means \pm S.E.M; $*p < 0.05$. (C) Diagram showing the timeline of i.p. injection of paclitaxel and sampling for ELISA. Mice were repeatedly i.p. injected with vehicle (16.7% ethanol) or paclitaxel (20 mg/kg) twice a week for 1–8 weeks. (D) Changes in score of paw withdrawal from a mechanical stimulus (0.16 g von Frey filament) in the right hindpaw of mice ($n = 7–11$). (E) Changes of plasma galectin-3 level in mice ($n = 3–6$). (F, G) Mice were repeatedly i.p. injected with vehicle (5% ethanol) or docetaxel (20 mg/kg) twice a week for 2 weeks. (F) Changes in score of paw withdrawal from a mechanical stimulus ($n = 8–9$). (G) Plasma galectin-3 concentration 2 weeks after the first injection. Data are means \pm S.E.M. $*p < 0.05$, $**p < 0.01$ and $***p < 0.001$ vs. the vehicle-treated group.

receiving weekly paclitaxel therapy (Patient No. 1 and 2). In a patient who received TC (Patient No. 7), the plasma galectin-3 level increased after the initiation of chemotherapy, although CIPN did not occur.

To better understand the relationship between the plasma galectin-3 levels and the development of CIPN, I next performed statistical analysis by classifying each galectin-3 concentration according to the presence or absence of CIPN. The plasma galectin-3 levels were significantly higher in the patients with CIPN (mean \pm SD: 8.190 ± 3.398 ng/mL) than before development of CIPN (5.703 ± 2.435 ng/mL) (Fig. 2-1B). Conversely, galectin-3 levels in the absence of CIPN were similar to those in subjects without cancer (5.353 ± 2.237 ng/mL, indicated by dashed line).

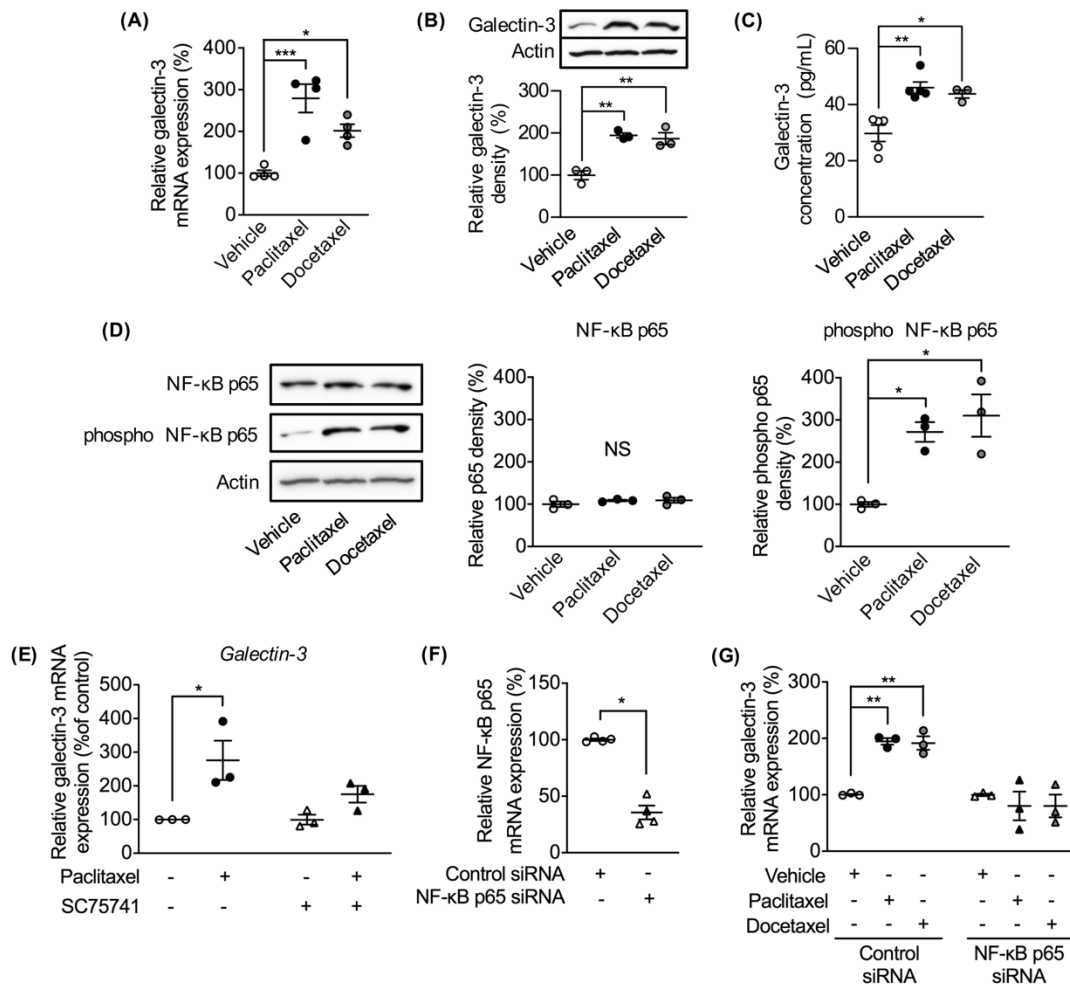


Fig. 2-2. Galectin-3 increases in dedifferentiated Schwann cell culture and is secreted extracellularly upon taxane treatment. (A–D) Schwann cells were treated with vehicle (0.1% DMSO), paclitaxel (10 nM), or docetaxel (10 nM) for 48 h. (A) Quantitative real-time RT-PCR analysis of *Galectin-3* mRNA expression in Schwann cells. $n = 4$. (B) Representative Western blots showing expression of galectin-3 and actin (*upper panels*), and quantification of band density (*lower graph*). Intensity of each band was normalized against that of actin (loading control). $n = 3$. (C) Galectin-3 concentration in the culture supernatant of Schwann cells, as determined by ELISA. $n = 3$ –5. (D) Representative Western blots showing NF- κ B p65, phosphorylated NF- κ B p65 (Ser536) and actin levels (*left panels*), and quantification of band density (*middle and right graphs*). $n = 3$. (E) Quantitative real-time RT-PCR analysis of *Galectin-3* mRNA expression. Schwann cells were treated with vehicle (0.1% DMSO) or paclitaxel (10 nM) in the presence or absence of the NF- κ B inhibitor SC75741 (1 μ M). $n = 3$. (F, G) After transfection with NF- κ B p65 siRNA or universal negative control siRNA, Schwann cells were treated with vehicle (0.1% DMSO), paclitaxel (10 nM) or docetaxel (10 nM) for 48 h. (F) Quantitative real-time RT-PCR analysis of *Nf- κ B p65* mRNA expression in Schwann cells treated with NF- κ B p65 siRNA. $n = 4$. (G) Quantitative real-time RT-PCR analysis of *Galectin-3* mRNA expression in siRNA-treated Schwann cells 48 h after treatment with vehicle (0.1% DMSO), paclitaxel (10 nM) or docetaxel (10 nM). $n = 3$. Data are expressed relative to the value in vehicle-treated cells (% of control) and are represented as means \pm S.E.M. * $p < 0.05$, ** $p < 0.01$ and *** $p < 0.001$ vs. the vehicle-treated group. N.S.: not significant.

Plasma galectin-3 level is elevated in a mouse model of taxane-related CIPN

Mice were i.p. injected with vehicle or paclitaxel (20 mg/kg) twice a week for 8 weeks,

and then subjected to analysis (Fig. 2-1C). Paclitaxel induced significant mechanical hypersensitivity in the hindpaw 2 weeks after the first injection relative to injection of vehicle alone (16.7% ethanol), and this effect persisted for 8 weeks (Fig. 2-1D). The plasma galectin-3 concentration increased in the paclitaxel-treated mice compared to the vehicle-administered mice from 1 to 4 weeks after the injection, reaching statistical significance 2 weeks after the first injection (Fig. 2-1E). Plasma galectin-3 recovered to the same level in the vehicle-treated group by 8 weeks after paclitaxel injection. Repeated injections of docetaxel (20 mg/kg, i.p.) also induced both significant mechanical hypersensitivity (Fig. 2-1F) and increased plasma galectin-3 levels (Fig. 2-1G) 2 weeks after the first injection.

Taxane treatment increases galectin-3 production and secretion from dedifferentiated Schwann cells

As shown in Chapter 1, treatment with paclitaxel (10 nM) or docetaxel (10 nM) for 48 h significantly increased *Galectin-3* mRNA (Fig. 2-2A) and protein levels (Fig. 2-2B) in Schwann cells. Furthermore, the 48 h treatment with either paclitaxel (10 nM) or docetaxel (10 nM) significantly increased the galectin-3 concentration in the supernatant of Schwann cells (Fig. 2-2C).

Galectin-3 expression is reported to be under the regulation of NF- κ B (51). I found that paclitaxel (10 nM) or docetaxel (10 nM) treatment significantly increased the level of phosphorylated NF- κ B p65 in Schwann cells, suggesting the activation of the NF- κ B signaling pathway (Fig. 2-2D). Co-treatment with a NF- κ B inhibitor, SC75741 (1 μ M), which inhibits NF- κ B binding to gene promoter regions (52), suppressed the paclitaxel-induced increase in the *Galectin-3* mRNA level (Fig. 2-2E). Similarly, NF- κ B p65 knockdown by specific siRNA significantly inhibited the increase in the *Galectin-3* mRNA level in taxane-treated Schwann cells (Fig. 2-2F, G).

Paclitaxel increases galectin-3 expression specifically in the neuroaxis of mouse sciatic nerve, but not in other organs or cells

To determine whether Schwann cell-derived galectin-3 could be the origin of plasma galectin-3 following paclitaxel administration, I evaluated the changes in galectin-3 expression in Schwann cells of the mouse sciatic nerve over a time course. The

experimental timeline and dose of paclitaxel were the same as described in Fig. 2-1C. Consistent with the elevation in the plasma galectin-3 level, the intensity of galectin-3-IR increased in the longitudinal section of the sciatic nerve from paclitaxel-injected mice from 2 to 4 weeks after injection, reaching significance at 2 weeks after the first administration of paclitaxel (Fig. 2-3A and C). The galectin-3-IR was almost completely co-localized with the IR of GFAP, which is a marker of Schwann cells (Fig. 2-3B). Likewise, expression of *Galectin-3* mRNA was significantly increased in the neuroaxis of the sciatic nerve, where Schwann cells are abundant, in paclitaxel-treated mice 2 and 4 weeks after the first injection (Fig. 2-3D). Repeated injection of paclitaxel for 2 weeks did not increase the *Galectin-3* mRNA level in the DRG, peripheral blood mononuclear cells (PBMCs), liver, heart, lung, small intestine, colon, or kidney (Fig. 2-3E).

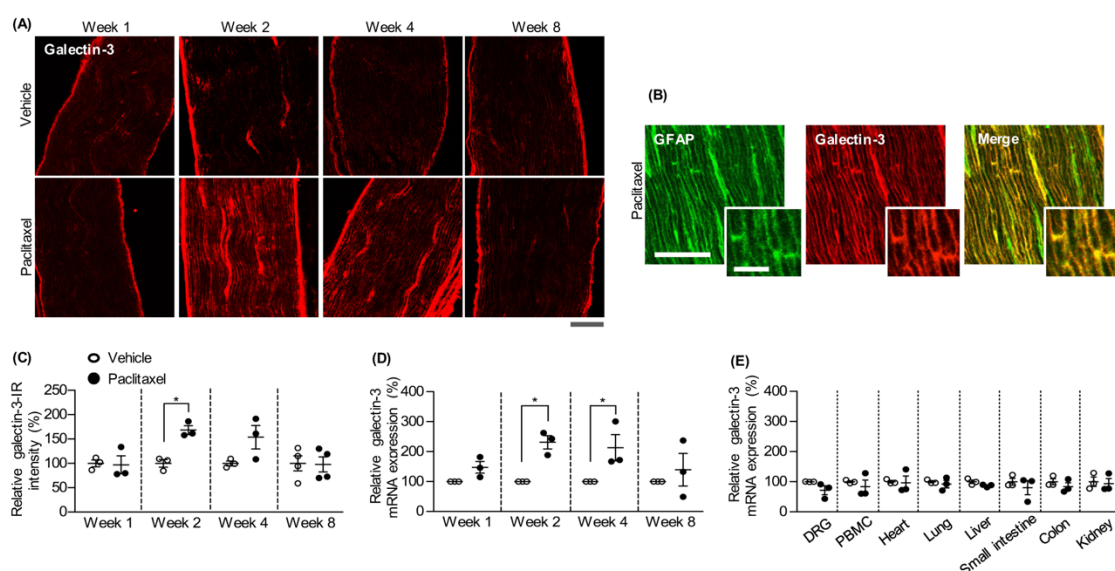


Fig. 2-3. Galectin-3 expression is increased only in the neuroaxis of the mouse sciatic nerve following paclitaxel administration. Mice were i.p. injected with vehicle (16.7% ethanol) or paclitaxel (20 mg/kg) twice a week for 1–8 weeks. **(A)** Representative confocal micrographs showing galectin-3 in a longitudinal section of sciatic nerve isolated from vehicle- or paclitaxel-injected mice. Scale bar: 100 μ m. **(B)** Representative confocal micrographs showing GFAP (green) and galectin-3 (red) in a longitudinal section of sciatic nerve isolated from paclitaxel-injected mice 2 weeks after the first injection. Enlarged images show the crowded area of the nodes of Ranvier. Scale bar: 100 μ m (25 μ m in the enlarged image). **(C)** Quantification of galectin-3-IR intensity in longitudinal sections of sciatic nerve isolated from vehicle- or paclitaxel-injected mice. $n = 3-4$. **(D)** Quantitative real-time RT-PCR analysis of *Galectin-3* mRNA expression in the neuroaxis of mouse sciatic nerve containing abundant Schwann cells. $n = 3$. **(E)** Quantitative real-time RT-PCR analysis of *Galectin-3* mRNA expression in DRG, PBMC, heart, lung, liver, small intestine, colon, and kidney, collected from vehicle- or paclitaxel-injected mice at 2 weeks after the first injection. $n = 3$. For quantification of *Galectin-3* mRNA expression, data are expressed relative to the vehicle-treated group (% of control). Data are means \pm S.E.M. * p < 0.05 vs. the vehicle-injected group.

Paclitaxel induces infiltration of macrophages into the mouse sciatic nerve

Given that galectin-3 serves as a chemoattractant for macrophages/monocytes (53,54), I hypothesized that Schwann cell-derived galectin-3 plays a critical role in macrophage infiltration leading to neuroinflammatory responses. As shown in Fig. 2-4A, repeated injection of paclitaxel significantly increased the number of Iba1-positive macrophages in the sciatic nerve 2 weeks after the first injection. The increased Iba1-positive cells decreased to the same level as the vehicle-treated control level by 8 weeks after paclitaxel injection (Fig. 2-4B).

To further investigate whether macrophages infiltrated the sciatic nerve after repeated injection of paclitaxel, I used BM chimeric mice derived by crossing donor C57BL/6GFP transgenic and recipient C57BL/6J mice. Reconstitution of pre-irradiated recipient mice with donor BM cells from GFP transgenic mice resulted in replacement of 98.2% of peripheral blood cells in recipient mice (*i.e.*, GFP-BM chimeric mice) by donor GFP-positive cells 6 weeks after transplantation (Fig. 2-4C). Repeated injection of paclitaxel increased GFP/Iba1-double positive cells (*i.e.*, GFP-BM-derived macrophages) in the sciatic nerves of GFP-BM chimeric mice (Fig. 2-4D). The number of GFP-positive cells in the sciatic nerve was significantly higher in paclitaxel-injected mice than in vehicle-injected mice (Fig. 2-4D). Furthermore, these increased GFP-positive macrophages in paclitaxel-treated GFP-BM chimeric mice were less co-localized with CD31-positive endothelial cells (Fig. 2-4E; white arrows), whereas GFP-positive cells in vehicle-treated mice were primarily adjacent to CD31-positive endothelial cells (Fig. 2-4E; white arrowheads), suggesting that BM-derived macrophages infiltrated the parenchyma of the sciatic nerve.

In addition, I investigated changes in the expression of pro- and anti-inflammatory macrophage-related genes, such as *Cd86* and *iNos* (a pro-inflammatory macrophage marker), *Irf5* (a transcription factor involved in pro-inflammatory macrophage polarization), *Il1 β* and *Tnfa* (pro-inflammatory cytokines), *Cd206* (an anti-inflammatory macrophage marker), *Irf4* (a transcription factor involved in anti-inflammatory macrophage polarization) and *Il10* (anti-inflammatory cytokines) in the mouse sciatic nerve 2 weeks after repeated paclitaxel injection. *iNos* mRNA expression was significantly increased in the sciatic nerve of paclitaxel-treated mice at 2 weeks after the first injection (Fig. 2-4F). Consistently, iNOS-IR was co-localized with Iba1-IR, and significantly increased in the mouse sciatic nerve (Fig. 2-4G). The repeated injection of

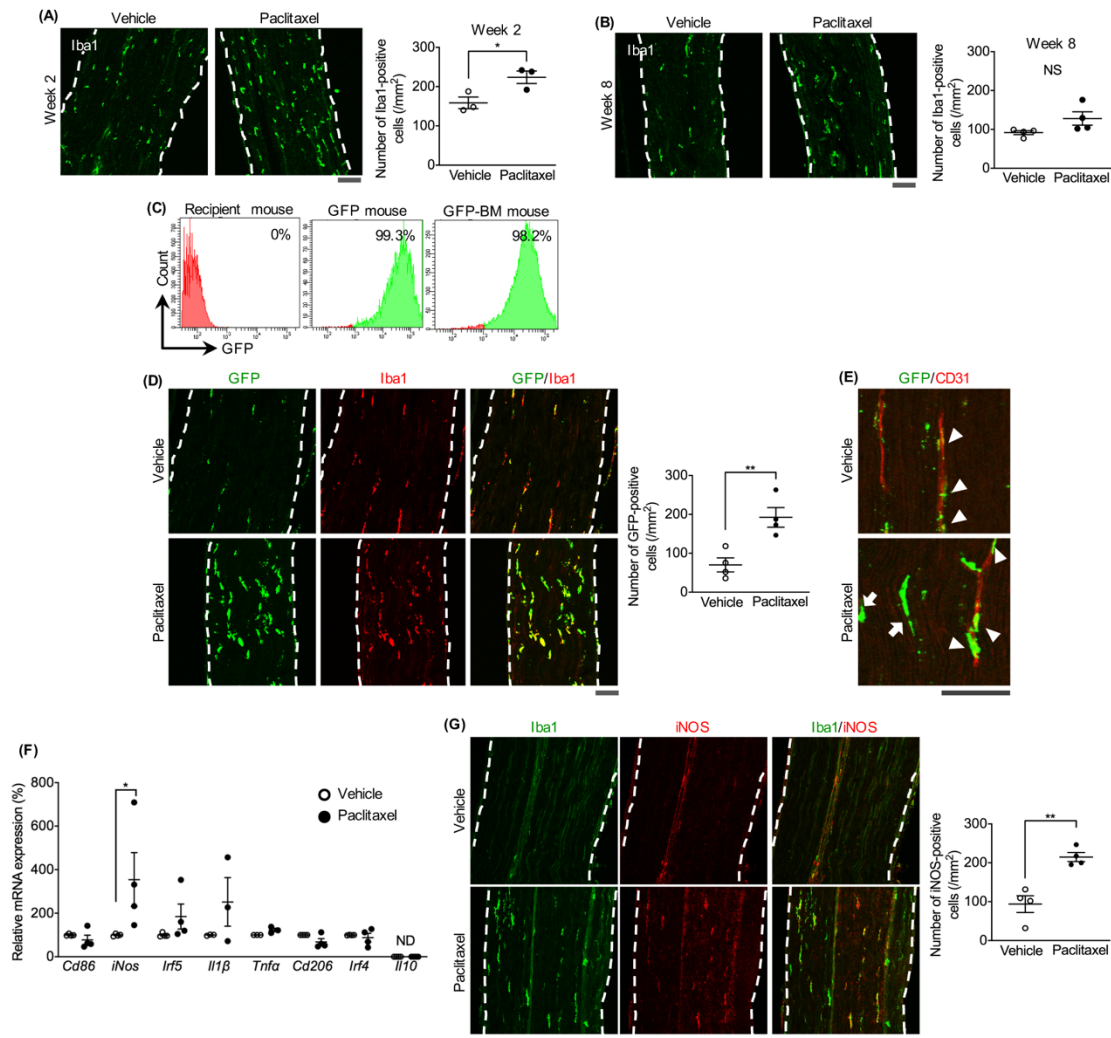


Fig. 2-4. Paclitaxel induces macrophage infiltration into the mouse sciatic nerve. C57BL/6J (A, B, F, G) or GFP-BM chimeric mice (D, E) were i.p. injected with vehicle (16.7% ethanol) or paclitaxel (20 mg/kg) twice a week for 1–8 weeks. (A, B) Representative confocal micrographs showing Iba1-IR (left panels) and number of Iba1-positive cells per mm² (right graphs) in the sciatic nerve. Immunohistochemistry was performed on longitudinal sections of mouse sciatic nerve at 2 (A) or 8 weeks (B) after the first injection of vehicle or paclitaxel. $n = 3-4$. N.S.: not significant. (C) Representative flow cytometry data of GFP-positive cells in BM-derived blood cells from C57BL/6J, GFP transgenic, and GFP-BM chimeric mice. C57BL/6J or GFP transgenic mice were used as GFP-negative or GFP-positive controls, respectively. Red and green peaks indicate the populations of GFP-negative and GFP-positive cells, respectively. (D, E) GFP-BM chimeric mice were i.p. injected with vehicle or paclitaxel twice a week for 2 weeks. (D) Representative confocal micrographs showing GFP fluorescence (green) and Iba1-IR (red) (left panel), and number of GFP-positive cells per mm² (right graph) in the sciatic nerve of a GFP-BM chimeric mouse. $n = 4$. (E) Representative confocal micrographs showing GFP fluorescence (green) and the endothelial cell marker CD31 (red) in the sciatic nerve of a GFP-BM chimeric mouse. Arrows and arrowheads indicate GFP-positive cells infiltrating the parenchyma or residing CD31-positive blood vessels, respectively. (F, G) Mice were i.p. injected with vehicle or paclitaxel twice a week for 2 weeks. (F) Quantitative real-time RT-PCR analysis of pro- and anti-inflammatory macrophage-related genes in the neuroaxis of sciatic nerve collected from vehicle- or paclitaxel-injected mice. $n = 3-4$. (G) Representative confocal micrographs showing Iba1- (green) and iNOS-IRs (red) (left panel), and number of iNOS-positive cells per mm² (right graph) in the mouse sciatic nerve. $n = 4$. Dotted lines in (A, B, D) and (G) indicate the outer edges of the sciatic nerve. Scale bars: 100 μ m. Data are means \pm S.E.M. * $p < 0.05$ and ** $p < 0.01$ vs. vehicle-injected group.

paclitaxel tended to increase the *Irf5* and *Il1 β* mRNA levels, but not that *Cd86*, *Tnfa*, *Cd206*, *Irf4*, or *Il10*, in the mouse sciatic nerve (Fig. 2-4F).

Perineural application of recombinant galectin-3 to the sciatic nerve induces the infiltration of macrophages and mechanical hypersensitivity in naive mice

In a chemotaxis assay, I observed significant migration of RAW 264.7 murine macrophage cells toward culture medium containing 2 pM rGalectin-3; this concentration was similar to that in culture supernatant of paclitaxel- or docetaxel-treated Schwann cells (see Fig. 2-2C; paclitaxel: 46.1 pg/mL = 1.77 pM, docetaxel: 43.8 pg/mL = 1.69 pM) (Fig. 2-5A). Furthermore, RAW 264.7 cells had a tendency of chemotactic responses toward culture supernatant freshly collected from Schwann cells treated with 10 nM paclitaxel for 2 days, although the effect was not statistically significant (Fig. 2-5B). The increase in the chemotactic response was completely abolished by addition of a neutralizing antibody against galectin-3 (10 μ g/mL) to culture supernatant from paclitaxel-treated Schwann cells (Fig. 2-5B). Perineural administration of 10 nM rGalectin-3 to the sciatic nerve significantly increased the number of Iba1-positive macrophages in the sciatic nerve of naive mice 3 and 7 days after application (Fig. 2-5C, D), and induced significant mechanical hypersensitivity (Fig. 2-5E).

Depletion of macrophages with clodronate inhibits paclitaxel-induced mechanical hypersensitivity

As shown in Fig. 2-5F, mice were i.p. injected three times with clodronate liposomes, a well-characterized macrophage-depleting compound (55), or control liposomes. Clodronate liposomes significantly decreased the number of Iba1-positive cells in the sciatic nerve of paclitaxel-injected mice relative to control liposomes (Fig. 2-5G, H). Consistent with this, clodronate liposomes significantly inhibited paclitaxel-induced mechanical hypersensitivity 2 weeks after injection (Fig. 2-5I). However, clodronate liposomes exacerbated the paclitaxel-induced increase in the plasma galectin-3 level, which was significantly higher than that in mice treated with control liposomes (Fig. 2-5J).

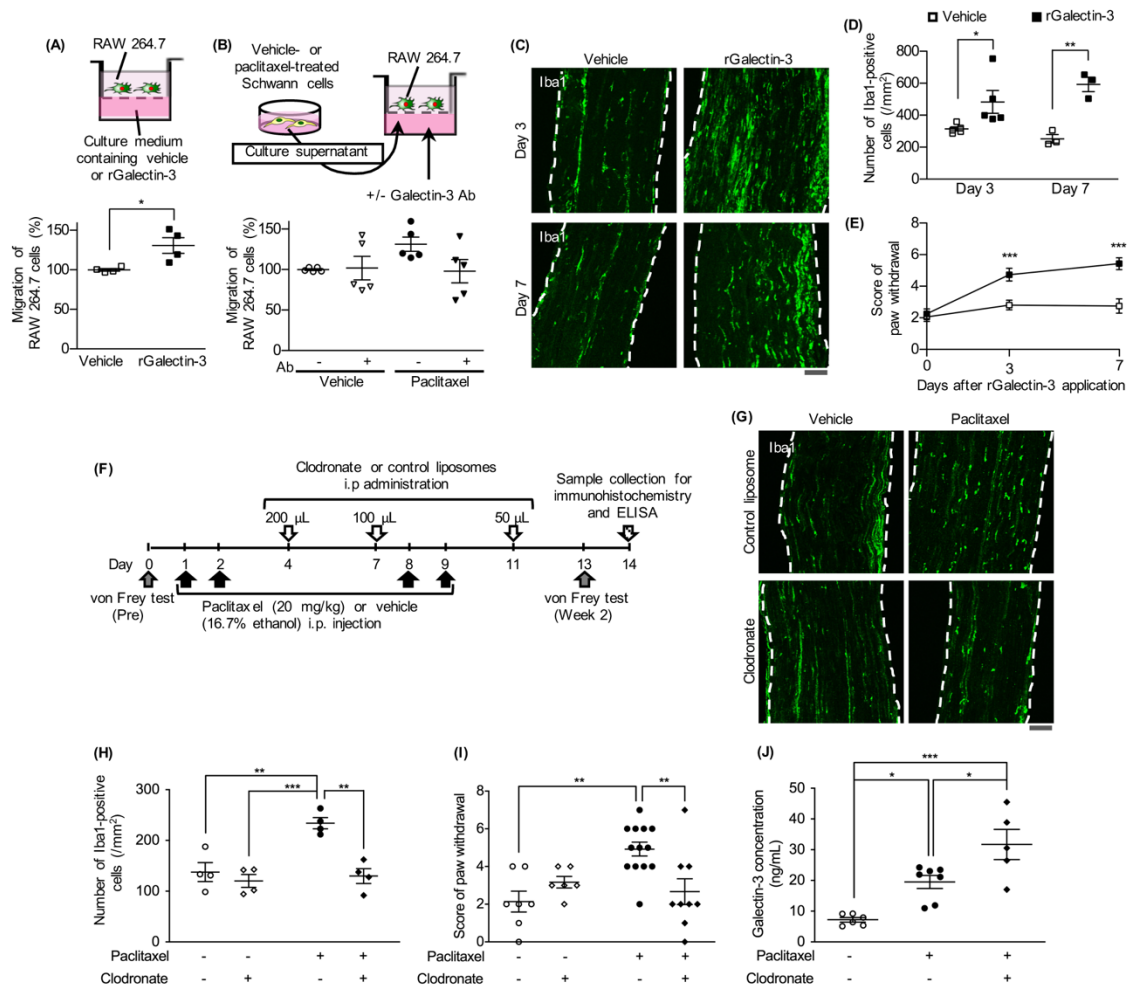


Fig. 2-5. Galectin-3 induces mechanical hypersensitivity via macrophage infiltration into the mouse sciatic nerve. (A) Migration of RAW 264.7 cells toward culture medium containing vehicle (PBS) or rGalectin-3 (2 pM). The value (Migration of RAW 264.7 cells [%]) is expressed relative to the data for the vehicle group (% of control). $n = 3$. (B) Migration of RAW 264.7 cells toward culture supernatant of vehicle- or paclitaxel-treated Schwann cells in the absence (Ab-) or presence (Ab+) of galectin-3 neutralizing antibody. Culture supernatant was freshly collected from Schwann cell cultures treated with vehicle (0.1% DMSO) or paclitaxel (10 nM) for 2 days, and 1.5 μ L of a galectin-3 neutralizing antibody (10 μ g/mL) or vehicle (PBS) was added into each sample. (C–E) rGalectin-3 (10 nM) or vehicle (PBS) was perineurally applied to the sciatic nerve of naive mice on day 0. Representative confocal micrographs showing Iba1-IR (C) and the number of Iba1-positive cells per mm² (D) in longitudinal sections of ipsilateral sciatic nerve 3 and 7 days after application of rGalectin-3 are shown. Dotted lines in (C) indicate the outer edges of the sciatic nerve. $n = 3–5$. Scale bar: 100 μ m. (E) Changes in score of paw withdrawal from a mechanical stimulus in the ipsilateral hindpaw of rGalectin-3- or vehicle-applied mice. $n = 7–16$. Data are represented as mean \pm S.E.M. * $p < 0.05$, ** $p < 0.01$, and *** $p < 0.001$. (F) Experimental diagram showing the timeline of i.p. injection of each drug, sample collection for immunostaining (G, H), von Frey test (I) and ELISA (J). Mice were i.p. injected with vehicle (16.7% ethanol) or paclitaxel (20 mg/kg) twice a week for 2 weeks, and injected three times with clodronate or control liposomes. (G, H) Representative confocal micrographs showing Iba1-IR (G) and the number of Iba1-positive cells per mm² (H) in longitudinal sections of the mouse sciatic nerve 2 weeks after the first paclitaxel injection. Dotted lines indicate the outer edges of the sciatic nerve. $n = 4$. Scale bar: 100 μ m. (I) Changes in score of paw withdrawal from a mechanical stimulus in the right hindpaw of mice 2 weeks after the first injection. $n = 6–13$. (J) Galectin-3 concentration in mouse plasma 2 weeks after the initiation of paclitaxel administration. $n = 5–7$. Data are represented as mean \pm S.E.M. * $p < 0.05$, ** $p < 0.01$, and *** $p < 0.001$.

Taxane-induced macrophage infiltration and mechanical hypersensitivity are suppressed in *Galectin-3*^{-/-} mice

To investigate whether lack of galectin-3 could influence paclitaxel-induced macrophage infiltration and mechanical hypersensitivity, I repeatedly injected wild-type (WT) and *Galectin-3*^{-/-} mice with vehicle (16.7% ethanol) or paclitaxel (20 mg/kg, i.p.) twice a week for 8 weeks. The increase in Iba1-positive macrophages observed in the sciatic nerve of paclitaxel-treated WT mice was significantly reduced in paclitaxel-treated *Galectin-3*^{-/-} mice 2 weeks after paclitaxel injection (Fig. 2-6A). Eight weeks after the injections, the levels of Iba1-IR in paclitaxel-injected WT and *Galectin-3*^{-/-} mice were similar to those in the corresponding vehicle-injected mice (Fig. 2-6B). The paclitaxel-induced mechanical hypersensitivity observed in the WT mice was also abolished in *Galectin-3*^{-/-} mice 1 and 2 weeks after injection (Fig. 2-6C). However, mechanical hypersensitivity gradually appeared in *Galectin-3*^{-/-} mice from 4 to 8 weeks after multiple

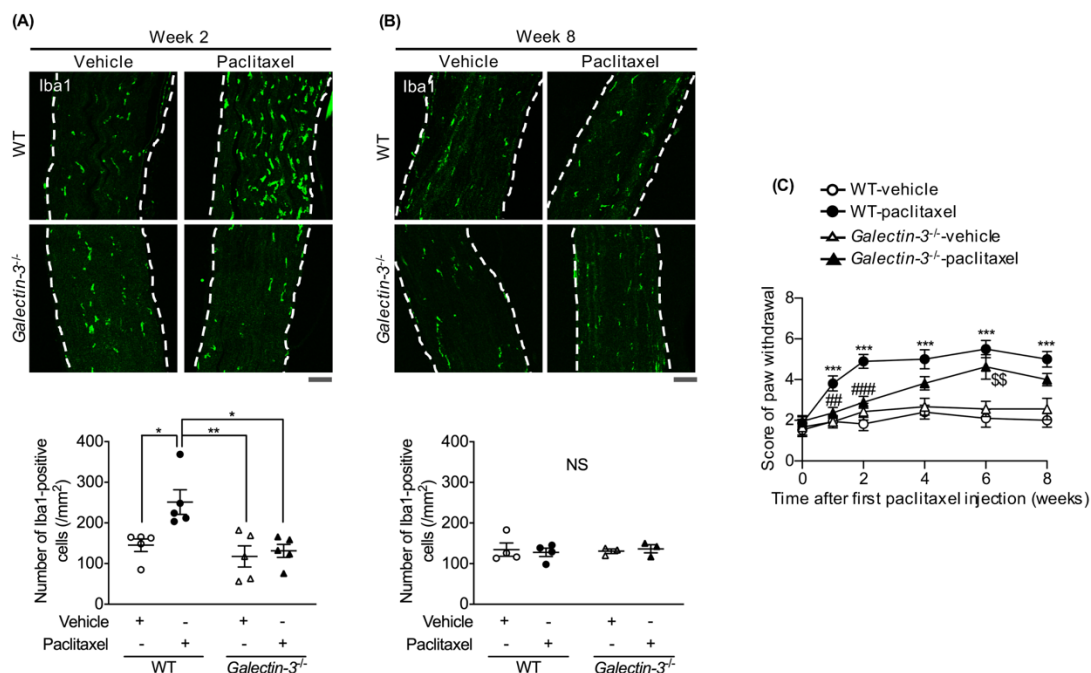


Fig. 2-6. Deficiency in galectin-3 inhibits paclitaxel-induced macrophage infiltration and mechanical hypersensitivity in mice. WT and *Galectin-3*^{-/-} mice were i.p. injected with vehicle (16.7% ethanol) or paclitaxel (20 mg/kg) twice a week for 1–8 weeks. (A, B) Representative fluorescence micrographs showing Iba1-IR (upper panels) and number of Iba1-positive cells per mm² (lower graphs) within longitudinal sections of the sciatic nerve of WT or *Galectin-3*^{-/-} mice 2 weeks (A) or 8 weeks (B) after the first injection. Dotted lines indicate the outer edges of the sciatic nerve. $n = 4-5$. Scale bars: 100 μm . Data are means \pm S.E.M. * $p < 0.05$, ** $p < 0.01$. N.S.: not significant. (C) Changes in score of paw withdrawal from a mechanical stimulus in the right hindpaw of WT or *Galectin-3*^{-/-} mice. $n = 7-22$. Data are means \pm S.E.M. *** $p < 0.001$, WT-vehicle vs. WT-paclitaxel; ## $p < 0.01$ and ### $p < 0.001$, WT-paclitaxel vs. *Galectin-3*^{-/-}-paclitaxel; \$\$ $p < 0.01$, *Galectin-3*^{-/-}-vehicle vs. *Galectin-3*^{-/-}-paclitaxel.

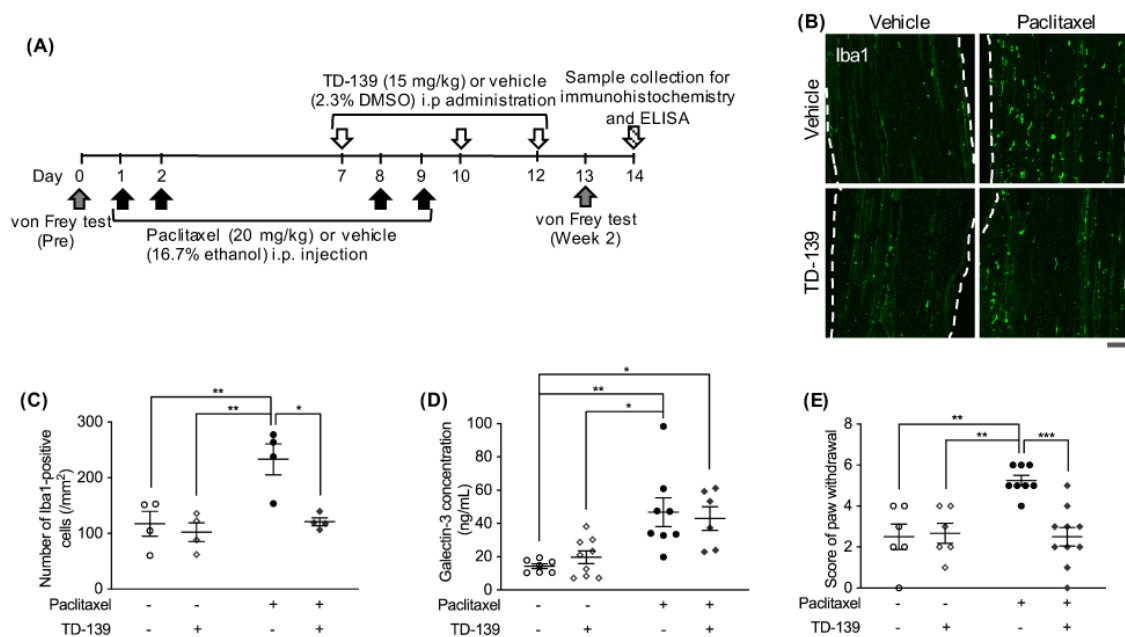


Fig. 2-7. The galectin-3 inhibitor TD-139 prevents paclitaxel-induced macrophage infiltration and mechanical hypersensitivity in mice. (A) Experimental diagram showing the timeline of i.p. injection of each drug, behavior test, immunostaining, and ELISA. (B, C) Representative confocal micrographs showing Iba1-IR (B) and number of Iba1-positive cells per mm² (C) in longitudinal sections of mouse sciatic nerve 2 weeks after the first paclitaxel injection. Dotted lines indicate the outer edges of the sciatic nerve. *n* = 4. Scale bar: 100 μ m. (D) Galectin-3 concentration in mouse plasma 2 weeks after the initiation of paclitaxel administration. *n* = 6–9. (E) Changes in score of paw withdrawal from a mechanical stimulus in the right hindpaw of mice 2 weeks after the first injection. *n* = 6–10. Data are means \pm S.E.M. **p* < 0.05, ***p* < 0.01, and ****p* < 0.001.

paclitaxel injections, and the extent of sensitivity was similar to that in paclitaxel-injected WT mice 6–8 weeks after injection.

The galectin-3 inhibitor TD-139 suppresses paclitaxel-induced macrophage infiltration and mechanical hypersensitivity

The galectin-3 inhibitor TD-139 (15 mg/kg) or vehicle (2.3% DMSO) was i.p. injected into mice for 3 times as indicated in Fig. 2-7A. TD-139 has high affinity for the carbohydrate recognition domain of galectin-3, and inhibits its binding to receptors and effector proteins (56). Treatment with TD-139 significantly suppressed macrophage infiltration into the mouse sciatic nerve 2 weeks after the first paclitaxel injection (Fig. 2-7B, C). By contrast, TD-139 did not affect the paclitaxel-induced increase in the plasma galectin-3 level (Fig. 2-7D). Under these conditions, paclitaxel-induced mechanical hypersensitivity was suppressed by TD-139 injection 2 weeks after paclitaxel injection (Fig. 2-7E).

Discussion

The first major finding of this study was that the plasma galectin-3 level was increased in both taxane-treated breast cancer patients accompanying CIPN and a mouse model of CIPN (as illustrated in Fig. 2-8). By contrast, the plasma galectin-3 level in taxane-treated breast cancer patients without CIPN was similar to that in non-cancer subjects. These results suggest that breast carcinoma has a minor effect, if any, on the plasma galectin-3 levels, and that the increase in the plasma galectin-3 level is related to the taxane-induced onset of CIPN. However, unlike breast cancer, high expression of galectin-3 is reported in other tissues, such as pancreatic, liver, and kidney cancer. Therefore, it remains possible that galectin-3 derived from these cancer types affects the blood galectin-3 levels in patients (57). Plasma galectin-3 was also elevated in CIPN model mice 2 weeks after repeated injections of taxanes, largely in parallel with the appearance of mechanical hypersensitivity. Thereafter, the elevated plasma galectin-3 level in paclitaxel-treated mice gradually decreased by 8 weeks after administration. Similarly, the average plasma concentration of galectin-3 among eight patients peaked 6 weeks after the beginning of chemotherapy. Taken together, these findings show that a transient increase in the plasma galectin-3 level is a pathological change related to CIPN that is common to humans and mice treated with taxanes.

Based on the data shown in Chapter 1 that taxanes increase galectin-3 expression in p75-positive dedifferentiated cells, I hypothesized that dedifferentiated Schwann cells residing in peripheral sensory nerves were the origin of elevated levels of plasma galectin-3 following taxane injection. To test this idea, I first quantitatively confirmed that paclitaxel and docetaxel treatment of primary cultures of mature Schwann cells induced galectin-3 upregulation. Under these conditions, galectin-3 secretion from Schwann cells was elevated after treatment with taxanes, suggesting that Schwann cells have the ability to secrete galectin-3 after dedifferentiation induced by taxanes. The increased expression of galectin-3 may be mediated through the NF- κ B signaling pathway, as reported previously in another type of cell (51). On the other hand, my results demonstrated that upregulation of galectin-3 in Schwann cells of the mouse sciatic nerve peaked around 2–4 weeks after the first paclitaxel injection, consistent with the elevation in the plasma galectin-3 level. By contrast, galectin-3 expression was not altered in DRG or other peripheral organs/cells expressing galectin-3, including heart, lung, liver, small intestine, colon, kidney, and PBMCs (including monocytes) (40,58,59) even after paclitaxel

injection. Additional studies are needed to elucidate the molecular mechanisms underlying dedifferentiation of Schwann cells induced by taxanes. Nonetheless, my data emphasize that the transient elevation of plasma galectin-3 in taxane-related CIPN model mice results from promotion of galectin-3 release from dedifferentiated Schwann cells. At present, I cannot convincingly explain why galectin-3 upregulation in the sciatic nerve peaked 2 weeks after taxane injection and decreased thereafter, even though mechanical hypersensitivity persisted. However, my data are essentially in agreement with a previous report showing that galectin-3 is rapidly induced in dedifferentiated Schwann cells in the PNS during Wallerian degeneration, but subsequently disappears within a week (60).

Consistent with previous reports (61,62), I found that paclitaxel-induced macrophage infiltration into the parenchyma of the sciatic nerve. Earlier studies documented that extracellular galectin-3 modulates immune reactions via chemotaxis of macrophages/monocytes (40,53). I demonstrated that the murine macrophage cell line RAW 264.7 exhibited a chemotactic response toward both recombinant galectin-3 and culture supernatant collected from paclitaxel-treated Schwann cells. Generally, macrophages infiltrate the sites of nerve injury and mature into the pro-inflammatory phenotype in response to microenvironment signals (63-65). The inflammatory factors produced by these macrophages in the PNS facilitate pain transmission from the periphery to the central nervous system (CNS) (46,64). Paclitaxel increased pro-inflammatory macrophage-related genes (*iNos*, *Irf5* and *Il1 β*) in the mouse sciatic nerve. A repeated injection of paclitaxel also increased iNOS-positive macrophages in the sciatic nerve, suggesting that infiltrated macrophages were polarized toward pro-inflammatory phenotype and thereafter may release IL1 β in the sciatic nerve. Furthermore, perineural administration of recombinant galectin-3 to the sciatic nerve of naive mice induced infiltration of macrophages and mechanical hypersensitivity. Overall, these results strongly suggest that Schwann cell-derived galectin-3 is an important determinant of macrophage infiltration into peripheral sensory nerves after paclitaxel administration.

I further demonstrated that *Galectin-3*^{-/-} mice exhibited delayed onset of paclitaxel-induced mechanical hypersensitivity relative to WT mice, accompanied by a lack of macrophage expansion in the sciatic nerve. In addition, the galectin-3 inhibitor TD-139 almost completely abolished paclitaxel-induced macrophage infiltration and mechanical hypersensitivity. Thus, my data reveal a pro-nociceptive role of extracellular galectin-3 in the development of taxane-related CIPN. Importantly, chemical depletion of

macrophages by clodronate liposomes suppressed paclitaxel-induced mechanical hypersensitivity, despite the higher level of plasma galectin-3. The findings do not exclude the possibility that galectin-3 acts directly on peripheral nerves during CIPN pathogenesis, but they do emphasize the central role of macrophages in the effects of galectin-3. Specifically, galectin-3 released from Schwann cells induces macrophage infiltration into the sciatic nerve, which promotes taxane-induced mechanical hypersensitivity (Fig. 2-8).

On the other hand, paclitaxel-induced mechanical hypersensitivity appeared gradually in *Galectin-3*^{-/-} mice, 4 to 8 weeks after multiple paclitaxel injections. Taken together with the transient upregulation of galectin-3 in the sciatic nerve and plasma, this observation suggests that galectin-3-induced macrophage infiltration is involved in the early phases of paclitaxel-induced peripheral neuropathy. It is widely accepted that one of major cause of taxane-related CIPN is pathological changes in sensory neurons due to neurotoxicity (66). Based on my findings, I speculate that direct impairment of sensory neurons by taxanes makes a major contribution specifically during later stages of taxane-induced peripheral neuropathy.

In conclusion, the data presented herein suggest that transient elevation of the plasma galectin-3 level is a CIPN-related pathological change common to humans and mice following taxane treatment. Extracellular galectin-3 derived from dedifferentiated Schwann cells in the sciatic nerve may be involved in the early phase, rather than the late phase, of taxane-induced mechanical hypersensitivity mediated by macrophage infiltration. Thus, drugs that inhibit the galectin-3 signaling axis between Schwann cells and macrophages have the potential to delay CIPN progression and prolong the duration of treatment with taxane-based chemotherapy.

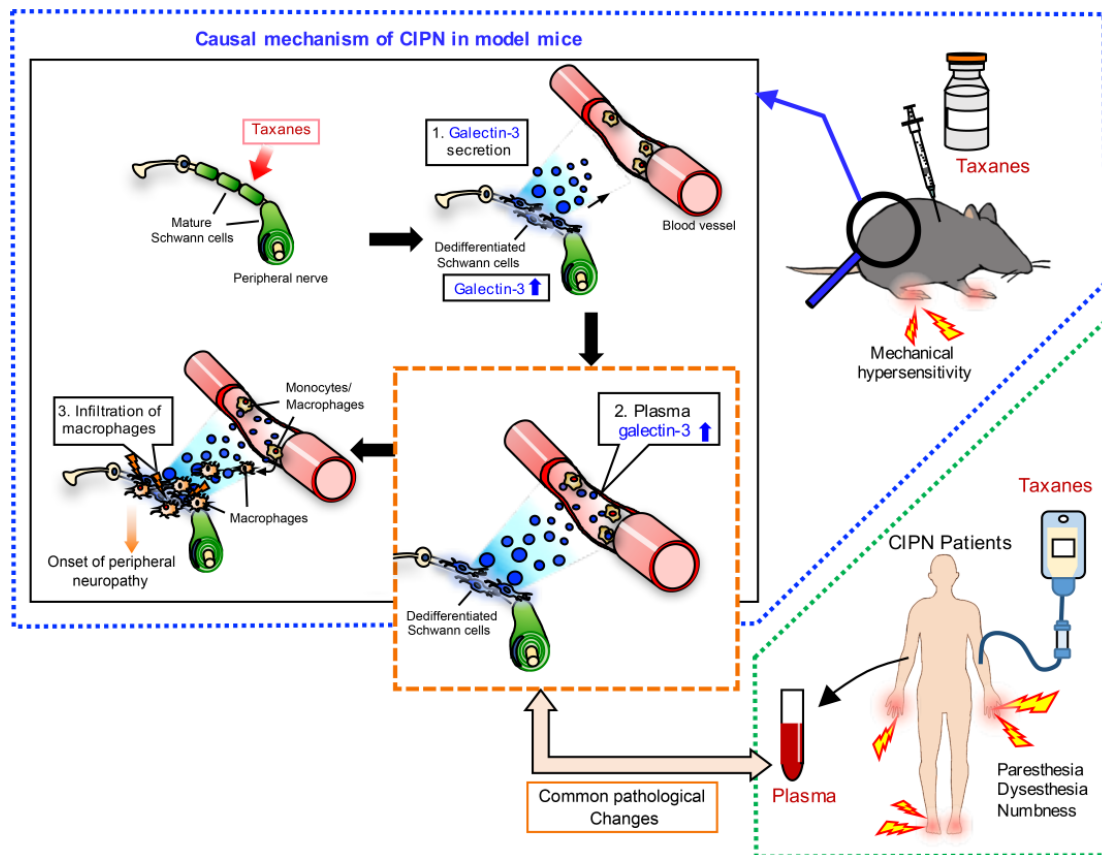


Fig. 2-8. Proposed mechanism of paclitaxel-induced peripheral neuropathy mediated by Schwann cell-derived galectin-3. In response to taxane treatment, mature Schwann cells (shown in green) transform into dedifferentiated Schwann cells (shown in blue) accompanied with galectin-3 upregulation. Galectin-3 (blue dots) is released from dedifferentiated Schwann cells, and in turn plasma galectin-3 level is elevated. Consequently, monocytes/macrophages (shown in orange) extravasate from the blood vessel into the peripheral nerves according to the concentration gradient of galectin-3. This Schwann cell-derived galectin-3 dependent macrophage infiltration could be involved in the onset of taxane-related peripheral neuropathy. Because the elevation of plasma galectin-3 level is the pathological change common to both taxane-related CIPN patients and model mice, the inhibition of this galectin-3 signaling could be new therapeutic strategy for taxane-related CIPN.

Chapter 3: Cilostazol is a causal therapy for preventing taxane-related CIPN by suppression of Schwann cell dedifferentiation

Introduction

Taxane-based chemotherapy must be completed without aggravation of CIPN because dose reduction, discontinuation, or delayed cycles of chemotherapy due to side effects can worsen disease-free or overall survival in cancer patients (67,68). Some analgesics (e.g., duloxetine, gabapentin, and pregabalin) that inhibit sensory pain transmission to the central nervous system (CNS) have been used as symptomatic treatment to relieve CIPN in clinic (69). However, the efficacy of these drugs against CIPN is limited (9,69): among these analgesics, only duloxetine was proven to have a significant effect on oxaliplatin-induced peripheral neuropathy in a randomized phase III study, but its efficacy on paclitaxel-related CIPN may be suspicious (70). Thus, despite the high medical need, no causal therapy has been approved for prevention or relief of CIPN, largely due to our insufficient understanding of the complex mechanisms underlying CIPN pathogenesis (8-10).

Oligodendrocytes, which form myelin sheaths in the CNS, are a new therapeutic target for treatment of multiple sclerosis (MS), an autoimmune demyelinating disease in the CNS (71). Supplementation of myelin-forming oligodendrocytes in lesion sites by induction of oligodendrocyte precursor cell (OPC) differentiation could be used as a causal therapy for this demyelinating disease (72-74). This idea is fascinating because it is theoretically applicable to the development of novel therapeutics for paclitaxel-related CIPN, as shown in Chapters 1 and 2, which is attributable to dedifferentiation of Schwann cells. Based on previous reports that intracellular cyclic adenosine monophosphate (cAMP) plays an essential role in Schwann cell differentiation (75,76), I hypothesized that phosphodiesterase (PDE) inhibitors, which increase the intracellular cAMP level, could alleviate paclitaxel-induced dedifferentiation of Schwann cells and thereby exert a therapeutic effect on paclitaxel-associated CIPN.

To this end, I screened several PDE inhibitors by immunocytochemical analysis in rat primary cultured Schwann cells and attempted to identify a novel candidate therapeutic for CIPN with the ability to differentiate Schwann cells. I found that a selective PDE3 inhibitor, cilostazol, potently inhibited paclitaxel-induced dedifferentiation of cultured Schwann cells via cAMP/exchange protein directly activated by cAMP (Epac) signaling,

and attenuated the mechanical hypersensitivity and dedifferentiation of Schwann cells within the sciatic nerve in a mouse model of paclitaxel-related CIPN.

Materials and Methods

Animals

All animal experiments were performed as described in Chapter 1. Pregnant Wistar/ST rats, male C57BL/6J JmsSlc (5–7 weeks) were obtained from Japan SLC.

Reagents

For *in vitro* experiments, cilostazol (Wako Pure Chemical Industries), KT5720 (Cayman Chemical, MI, USA), and ESI-09 (Sigma-Aldrich) were prepared as stock solutions in DMSO at concentrations of 50 mM, 10 mM, and 10 mM, respectively. 8-Bromo-cAMP (Tocris Bioscience, UK) was dissolved in distilled water as a stock solution at a concentration of 100 mM. Concentrations of stock solutions used in drug screening are listed in Table 3-1. The stock solutions were stored at -30°C.

For *in vivo* experiments, paclitaxel solution (30 mg/5mL), which was containing ~50% ethanol, was purchased from Nippon Kayaku (Tokyo, Japan). This paclitaxel was diluted to 0.5 mg/mL with saline for i.p. injection (i.e., 5 mg/kg per 1 mouse, i.p.). Because ~4.2% ethanol was present in the dilute solution of paclitaxel, saline containing ethanol at the same concentration was used as the vehicle. Diet containing 0.3% (w/w) cilostazol was manufactured by Oriental Yeast (Tokyo, Japan). Chow containing 0.3% cilostazol has been widely administered to rats and mice in previous studies of the effect of cilostazol (77,78).

Quantitative analysis by real-time RT-PCR

PCR was performed as described in Chapter 1. Details of synthesized primers are described in Table 3-2.

CIPN model

Male C57BL/6J mice were i.p. injected with paclitaxel (5 mg/kg) or vehicle (4.2% ethanol) twice a week (on day 1 and 2) for a total of 1–8 weeks. For cilostazol administration, mice were continuously and freely fed a diet containing 0.3% cilostazol

starting 1 day before the first paclitaxel or vehicle injection until just before sample collection.

von Frey filament test (up-down method)

Mechanical sensitivity was evaluated as described in Chapter 1.

Tumor cell culture

The human breast cancer cell line MDA-MB-231 (ATCC, Manassas, VA, USA; RRID: CVCL_0062) was maintained in 100 mm culture dishes containing Leibovitz's L-15 medium (ATCC) supplemented with 10% FBS and 1% penicillin–streptomycin at 37°C in a humidified atmosphere without CO₂.

Viability assay of MDA-MB-231 cells

MDA-MB-231 cells were seeded in 24 well plates. After 2 days of culture, the cells were treated with vehicle (0.1% DMSO) or paclitaxel (10 nM) in the presence or absence of cilostazol (30 μM) for 48 h. MTT assay was performed as described in Chapter 1.

Statistics

Data are presented as means ± S.E.M. and were analyzed using GraphPad Prism version 8.0. Data from more than two groups were compared using a one-way or two-way ANOVA, followed by Tukey's multiple comparisons test. Statistical analyses of 50% withdrawal thresholds in the von Frey filament test were performed using the Kruskal–Wallis test followed by Dunn's multiple comparison test for each week. In all cases, $p < 0.05$ was considered statistically significant.

Other experiments were performed as described in Chapter 1.

Table 3-1. Information about drugs used in screening

Drug	Source, Catalog no.	Stock solution
Cilostazol	Wako Pure Chemical Industries, Cat# 038-20661	50 or 100 mM in DMSO
Dipyridamole	Sigma-Aldrich, Cat# D9766	50 mM in DMSO
Rolipram	Wako Pure Chemical Industries, Cat# 180-01411	100 mM in DMSO
Sildenafil	Wako Pure Chemical Industries, Cat# 192-16683	10 mM in DMSO
Theophylline	Wako Pure Chemical Industries, Cat# 209-09932	100 mM in DMSO
Benzotropine	MP Biomedicals, Cat# 153626	100 mM in DMSO
Gabapentin	Wako Pure Chemical Industries, Cat#: 076-05641	100 mM in distilled water

Table 3-2. Sequences of synthesized primers used in PCR assays

Target name		Primer sequence	GenBank sequence accession number
<i>p75</i>	Sense	5'-GCT GGG TTA CCA GCC TGA AC-3'	NM_012610
	Antisense	5'-GCA GTG GAC TCG CTG CAT AG-3'	
<i>PDE3</i>	Sense	5'-CCT GCA CCT GAT GAC CAA GA-3'	AH000839.1
	Antisense	5'-GCT CGT CAA GGG GAA TTT CA-3'	
<i>PDE4</i>	Sense	5'-CTC TAC GCC AGC ACT GGA TG-3'	M25350.1
	Antisense	5'-GTG TCT GGC GTT GCT TCT TG-3'	
<i>PDE5</i>	Sense	5'-CAA GGG AGC TCC AGG CTC TA-3'	U76032.1
	Antisense	5'-TCC ATC GGC AAA GAA CCT CT-3'	
<i>PDE6</i>	Sense	5'-AAT CAA ATT CGA GCG GAG GA-3'	NM_142112.5
	Antisense	5'-TAG CGG TGG CAT GGT AAC TG-3'	
<i>MBP</i>	Sense	5'-GAA GCC AGG ATT TGG CTA CG-3'	NM_001025291
	Antisense	5'-CAG AGC GGC TGT CTC TTC CT-3'	
<i>Galectin-3</i>	Sense	5'-GAC ATC GCC TTC CAC TTT AAC C-3'	NM_031832.1
	Antisense	5'-GTC TTT CTT CCC TTC CCC AGT T-3'	
<i>GAPDH</i>	Sense	5'-GTT ACC AGG GCT GCC TTC TC-3'	NM_017008
	Antisense	5'-TGA TGA CCA GCT TCC CAT TC-3'	

Results

Dedifferentiated Schwann cells revert to mature state after washout of paclitaxel

After 48 h of culture in differentiation medium, rat primary cultured Schwann cells were exposed to vehicle (0.1% DMSO) or paclitaxel (10 nM) for 48 h, and then the culture medium was removed from cells and replaced with vehicle-containing differentiation medium (washout of paclitaxel). Treatment of mature Schwann cells with paclitaxel (10 nM) for 48 h increased the p75-IR level and caused marked morphological changes, compared to vehicle-treated cells, characterized by retraction of bipolar processes and a rounded shape (Fig. 3-1A). Real-time RT-PCR analysis also revealed a significant increase in *p75* mRNA in Schwann cells (Fig. 3-1C). The elevated expression of p75 and morphological changes in paclitaxel-treated cells reverted 48 h after washout of paclitaxel (Fig. 3-1B, C).

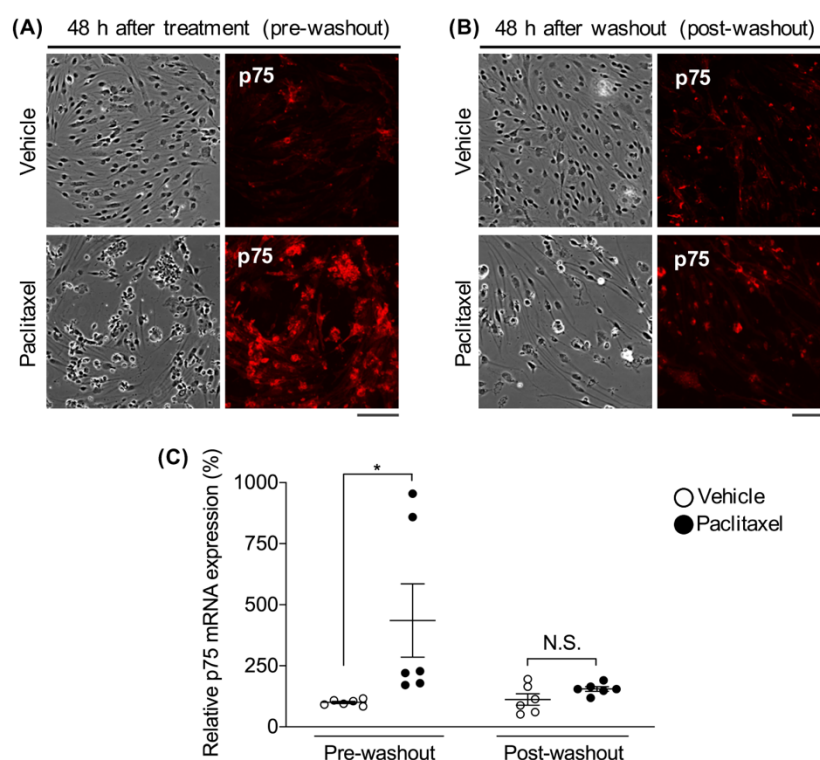


Fig. 3-1. Paclitaxel-induced dedifferentiated Schwann cells revert to the mature state after the washout of paclitaxel. Schwann cells were treated with vehicle (0.1% DMSO) or paclitaxel (10 nM) for 48 h. Then, the culture medium was removed and replaced with vehicle-containing differentiation medium. (A, B) Representative confocal micrographs showing phase and p75 (red) at 48 h after the drug treatment (pre-washout, A) or 48 h after the washout of paclitaxel (post-washout, B) in Schwann cells. Scale bars: 100 μ m. (C) Quantitative real-time RT-PCR analysis of *p75* mRNA expression at pre- or post-washout. $n = 6$. Data are expressed relative to the value in vehicle-treated cells (% of control) and are represented as means \pm S.E.M. * $p < 0.05$. NS: not significant.

Cilostazol promotes Schwann cell differentiation

Given that Schwann cells can spontaneously redifferentiate after removal of paclitaxel, I hypothesized that a drug that accelerates the transition of Schwann cells into the mature state could prevent paclitaxel-induced Schwann cell dedifferentiation. Consistent with previous reports showing that the differentiation process of Schwann cells is regulated by a cAMP-dependent pathway (75,76), I confirmed that exposure of immature Schwann cells to the cell-permeable cAMP analog 8-bromo-cAMP (1 mM) for 48 h increased the level of MBP-IR and decreased the level of p75-IR, a pattern similar to that observed in mature Schwann cells (Fig. 3-2A). In addition, I observed expression of *PDE3*, *PDE4*, and *PDE5* mRNAs in immature Schwann cells and vehicle (0.1% DMSO)- or paclitaxel (10 nM)-treated mature Schwann cells (Fig. 3-2B). *PDE6* mRNA was not detected in Schwann cells, regardless of differentiation status. Using these cells, I screened inhibitors of PDE3 (cilostazol), PDE4 (rolipram), and PDE5 (sildenafil), as well as non-selective PDE inhibitors (theophylline and dipyridamole) and other candidate drugs to examine whether they can induce differentiation of Schwann cells (Fig. 3-2C, Supplemental Fig. 3-1 and Table 3-1). For the screening, immature Schwann cells were treated with vehicle-containing maintenance medium as a negative control (immature Schwann cells), vehicle-containing differentiation medium as a positive control (mature Schwann cells), or each candidate diluted in maintenance medium at the final concentration shown in Fig. 3-2C and Supplemental Fig. 3-1. After a 48 h incubation, based on the intensity of p75- or MBP-IR in the negative control group (indicated by a dark blue circle in Fig. 3-2C), the degree of p75-IR reduction [p75 suppression ratio (%)] or MBP-IR increase [MBP induction ratio (%)] in the positive control group was defined as 100% (indicated by a red circle in Fig. 3-2C). Then, the p75-IR reduction and MBP-IR increase in individual PDE inhibitor-treated groups were calculated, and the data were plotted (Fig. 3-2C).

Among the five PDE inhibitors examined, cilostazol (10, 30, 50 and 100 μ M) caused a concentration-dependent increase in the MBP-IR at 10, 30, and 50 μ M and a decrease in the p75-IR at 10 and 30 μ M (CL; green circles in Fig. 3-2C). Sildenafil (0.1, 1, 3 and 10 μ M) also induced Schwann cell differentiation with a maximum effect at 10 μ M (SD; orange circles in Fig. 3-2C and Supplemental Fig. 3-1). Dipyridamole exerted a mild effect on Schwann cell differentiation at 10 μ M (DP; a magenta circle in Fig. 3-2C and Supplemental Fig. 3-1) and induced cytotoxicity at higher concentrations (data not shown). Although rolipram (RL; 10, 30 and 100 μ M, brown circles) and theophylline

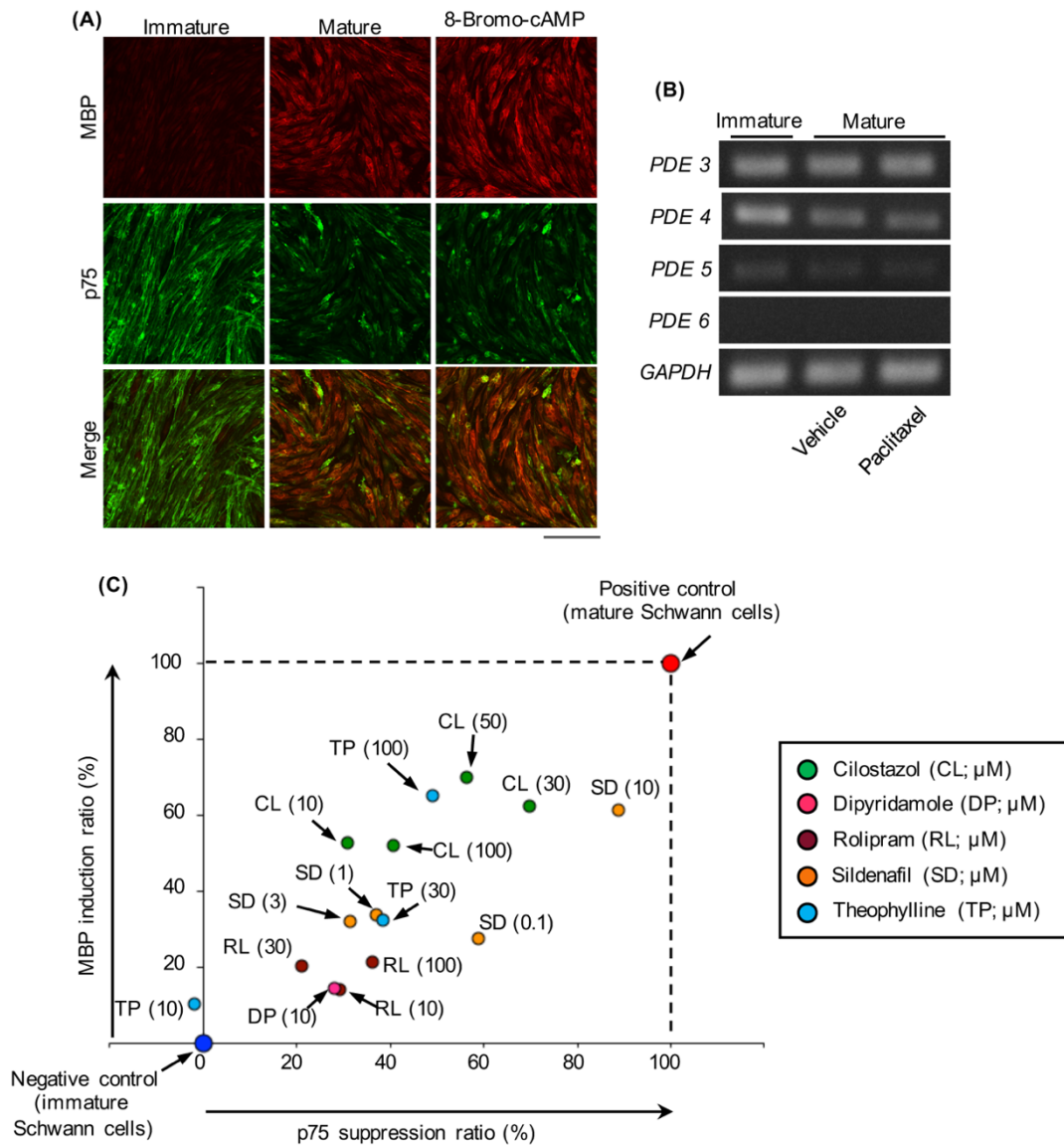


Fig. 3-2. Cilostazol is a potent inducer of Schwann cell differentiation. (A) Representative confocal micrographs showing MBP- (red) and p75-IRs (green) in primary cultures of rat Schwann cells. Immature Schwann cells were incubated in maintenance medium (Immature), differentiation medium (Mature), or maintenance medium containing 8-bromo-cAMP (1 mM) for 48 h. Scale bar: 100 μ m. (B) Representative RT-PCR bands showing expression of *PDE3*, *PDE4*, *PDE5*, and *PDE6* mRNA in immature (left lane), vehicle-treated (0.1% DMSO; middle lane), or paclitaxel-treated (10 nM; right lane) mature Schwann cells. *GAPDH* was used as an internal control. (C) Scatter plot showing results of screening for five PDE inhibitors based on immunocytochemical analyses. Immature Schwann cells were treated with vehicle-containing maintenance medium as a negative control (i.e., immature Schwann cells), vehicle-containing differentiation medium as a positive control (i.e., mature Schwann cells), or the indicated drug diluted in maintenance medium at the final concentration shown in the graph. After a 48 h incubation, cells were immunostained for MBP and p75. Based on the intensity of p75- or MBP-IR in the negative control group (indicated by a dark blue circle), the % decrease in the p75-IR [p75 suppression ratio (%)] or increase in the MBP-IR [MBP induction ratio (%)] in the positive control group was defined as 100% (indicated by a red circle). Similarly, the % decrease in p75-IR or increase in MBP-IR in each PDE inhibitor-treated group was calculated based on the intensity of p75- or MBP-IR in the negative control group. Each color circle indicates the average value of three samples.

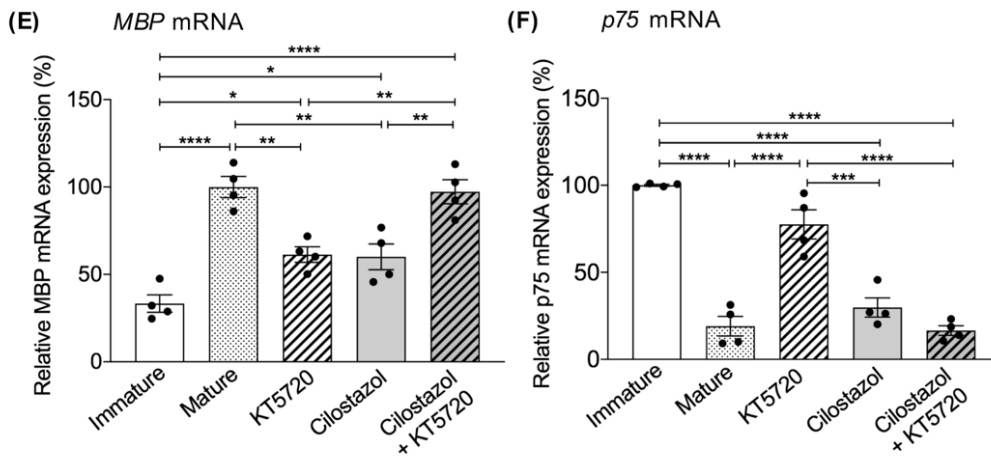
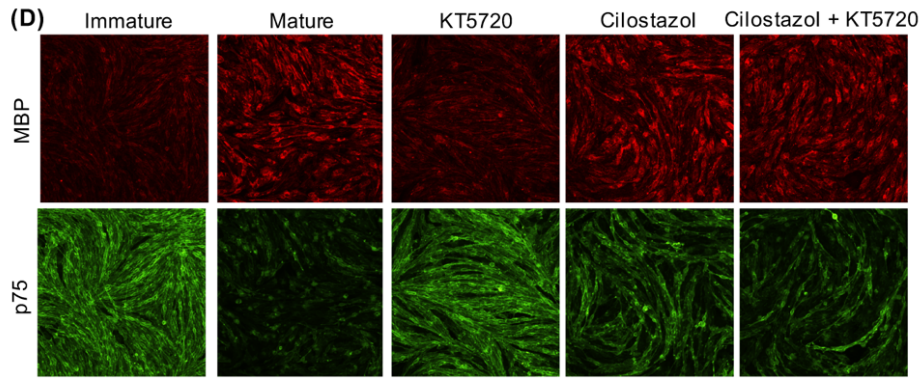
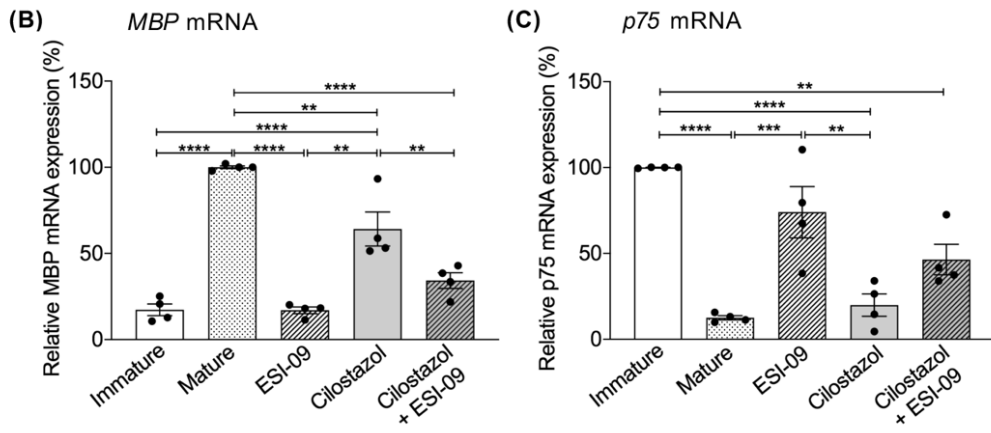
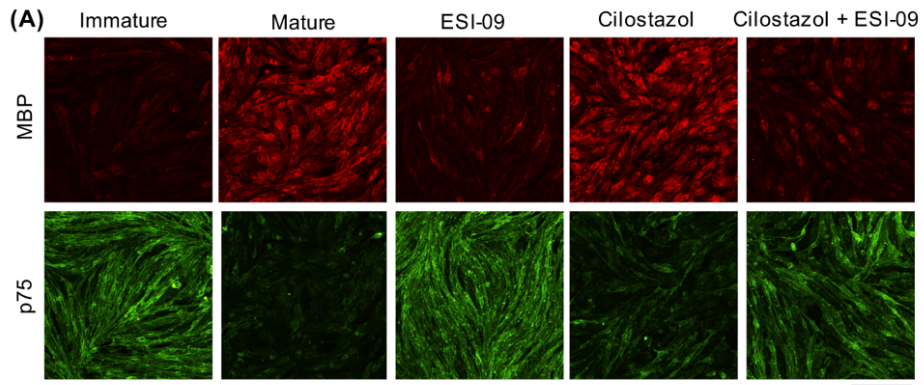


Fig. 3-3. Cilostazol-induced Schwann cell differentiation is mediated through cAMP/Epac signaling but not cAMP/PKA signaling. Immature Schwann cells were incubated for 48 h in maintenance medium (Immature), differentiation medium (Mature), or maintenance medium containing cilostazol (30 μ M) in the presence or absence of the Epac inhibitor ESI-09 (1 μ M, **A–C**) or the PKA inhibitor KT5720 (0.1 μ M, **D–F**). (**A, D**) Representative confocal micrographs showing MBP- (red) and p75-IRs (green) in Schwann cells. Scale bar: 100 μ m. (**B, C, E, F**) Quantitative real-time RT-PCR analysis of *MBP* (**B, E**) or *p75* (**C, F**) mRNA expression. $n = 4$.

(TP; 10, 30 and 100 μ M, light blue circles) increased MBP-IR and decreased p75-IR in Schwann cells, these effects were much weaker than those of cilostazol (Fig. 3-2C and Supplemental Fig. 3-1). Benztropine is a novel MS therapeutic candidate with the ability to differentiate OPCs in the CNS (72), but this did not induce differentiation of immature Schwann cells (Supplemental Fig. 3-1). Gabapentin is an analgesic widely used for neuropathic pain and has also been reported to differentiate OPCs in the CNS (72), but it only slightly increased MBP-IR in Schwann cells, even at a considerably higher dose (1 mM) (Supplemental Fig. 3-1). Based on these screening results, I selected cilostazol as a candidate drug and took 30 μ M as the optimal concentration for inducing Schwann cell differentiation. Sildenafil also exhibited a strong ability to induce Schwann cell differentiation, but was excluded from the list of candidates due to its short half-life in human (79).

Cilostazol induces Schwann cell differentiation via cAMP/Epac signaling

Cilostazol increases the intracellular cAMP level by inhibiting PDE3 activity (80). As cAMP activates two main effectors, protein kinase A (PKA) and Epac (81), I sought to identify the downstream signaling effector in cilostazol-induced Schwann cell differentiation. To this end, I used a PKA inhibitor (KT5720) and an Epac inhibitor (ESI-09) (Fig. 3-3). As in mature Schwann cells, treatment with cilostazol (30 μ M) increased MBP-IR and decreased p75-IR in immature Schwann cells. In parallel with the changes in the IRs, the cilostazol treatment (30 μ M) upregulated *MBP* mRNA and downregulated of *p75* mRNA. As shown in Fig. 3-3A–C, the cilostazol-induced changes in the levels of IRs and mRNAs of MBP and p75 were suppressed in the presence of ESI-09 (1 μ M). Treatment with ESI-09 alone had no effect on the differentiation status of immature Schwann cells. By contrast, KT5720 (0.1 μ M) appeared to enhance, rather than suppress, the effects of cilostazol on Schwann cells (Fig. 3-3D–F). Treatment with KT5720 alone induced significant increase in the *MBP* mRNA level, but did not change the *p75* mRNA level compared to immature Schwann cells.

Cilostazol prevents paclitaxel-induced dedifferentiation of cultured Schwann cells

I next examined whether cilostazol could prevent paclitaxel-induced Schwann cell dedifferentiation. For this purpose, Schwann cells were exposed to paclitaxel (10 nM) in the presence or absence of cilostazol (30 μ M) for 48 h, and subsequently cultured in maintenance medium containing vehicle (0.1% DMSO) or cilostazol (30 μ M) for 24 h as a recovery period. Paclitaxel treatment without cilostazol for 48 h followed by culture in vehicle-containing medium significantly decreased the MBP-IR, and increased p75- and galectin-3-IRs, in cultured Schwann cells relative to the vehicle-treated group. These paclitaxel-induced changes were almost completely suppressed by co-treatment with cilostazol (Fig. 3-4A–D). Immunocytochemical data were complemented by real-time

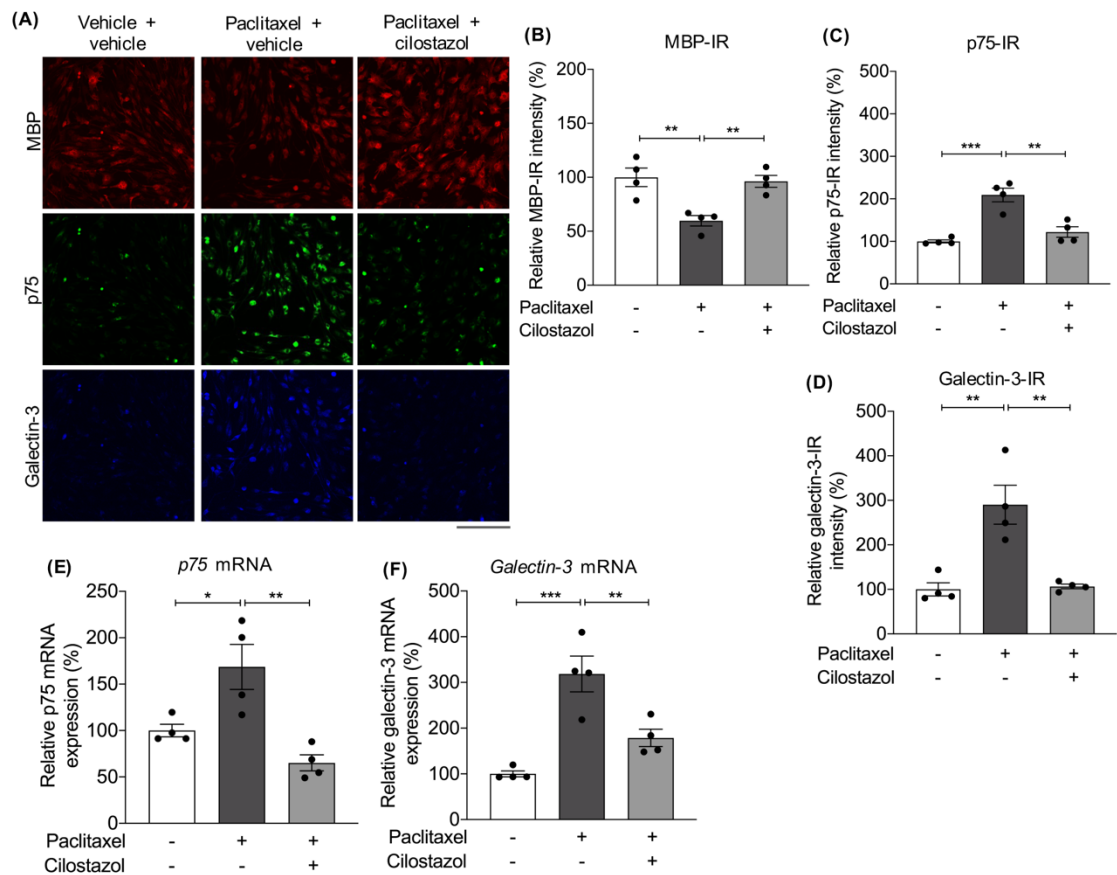


Fig. 3-4. Cilostazol prevents paclitaxel-induced Schwann cell dedifferentiation. Mature Schwann cells were treated with vehicle (0.1% DMSO) or paclitaxel (10 nM) in the presence or absence of cilostazol (30 μ M) for 48 h, and then the culture medium was removed and cultured in fresh maintenance medium containing vehicle or cilostazol for 24 h as a recovery period. **(A)** Representative confocal micrographs showing MBP (red), p75 (green), or galectin-3 (blue) in Schwann cells. Scale bar: 100 μ m. **(B–D)** Quantification of intensity of MBP-IR, p75-IR, or galectin-3-IR in Schwann cells. $n = 4$. **(E, F)** Quantitative real-time RT-PCR analysis of *p75* or *Galectin-3* mRNA expression. $n = 4$. Data are expressed relative to the value in vehicle-treated cells (% of control) and are represented as means \pm S.E.M. * $p < 0.05$, ** $p < 0.01$, and *** $p < 0.001$.

RT-PCR analysis. The increases in the expression levels of *p75* and *Galectin-3* mRNA in paclitaxel-treated Schwann cells were significantly suppressed by the cilostazol co-treatment (Fig. 3-4E and F).

Cilostazol prevents paclitaxel-induced demyelination in a mixed culture of Schwann cells and DRG neurons

I next investigated the effect of cilostazol on paclitaxel-induced demyelination by performing *in vitro* myelination experiments (Fig. 3-5). In a mixed culture of Schwann cells and DRG neurons, Schwann cells differentiated along DRG axons and eventually formed MBP-positive myelin segments, as indicated by the apparent overlap of MAP2- and MBP-IRs. Treatment with paclitaxel (10 nM) in the absence of cilostazol led to a significant reduction in MBP-IR, implying loss of myelinating Schwann cells from the co-cultures. Co-treatment with cilostazol (30 μ M) and paclitaxel for 48 h significantly prevented the paclitaxel-induced reduction in MBP-IRs. I did not observe significant differences between the groups in MAP2-positive neural axons.

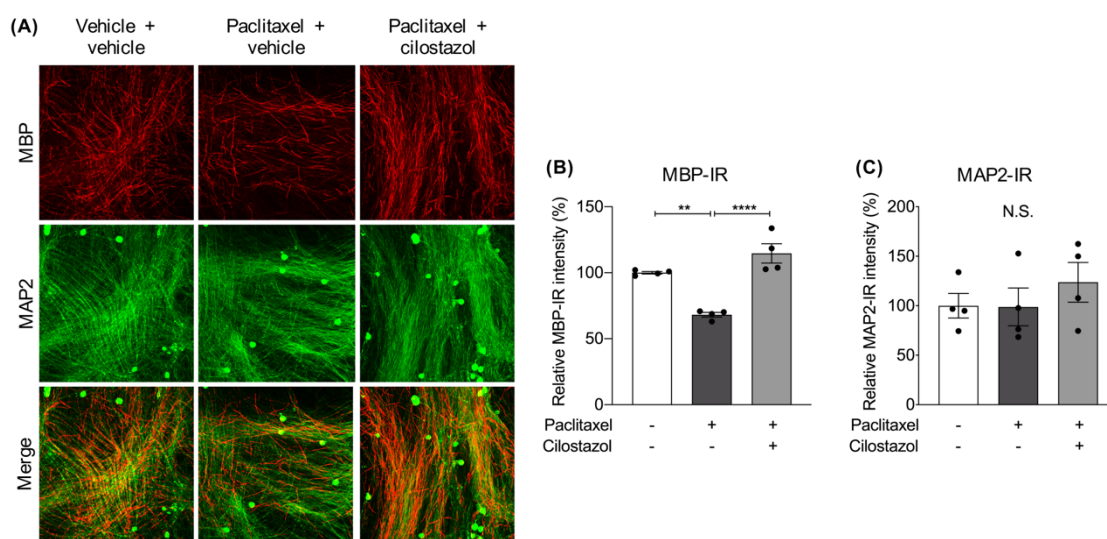


Fig. 3-5. Cilostazol suppresses paclitaxel-induced demyelination in Schwann cell/DRG neuron co-cultures. Schwann cell/DRG neuron co-cultures were treated with vehicle (0.1% DMSO) or paclitaxel (10 nM) in the presence or absence of cilostazol (30 μ M). After 48 h, the culture medium was removed, and the cells were cultured for 24 h in fresh medium containing vehicle or cilostazol as a recovery period. (A) Representative confocal micrographs showing MBP- (red) and MAP2-IRs (green) in Schwann cell/DRG neuron co-cultures. Scale bar: 200 μ m. (B, C) Quantification of intensity of MBP-IR or MAP2-IR. $n = 4$. Data are expressed relative to the value in vehicle-treated cells (% of control) and are represented as means \pm S.E.M. * $p < 0.05$ and ** $p < 0.01$. N.S.: not significant.

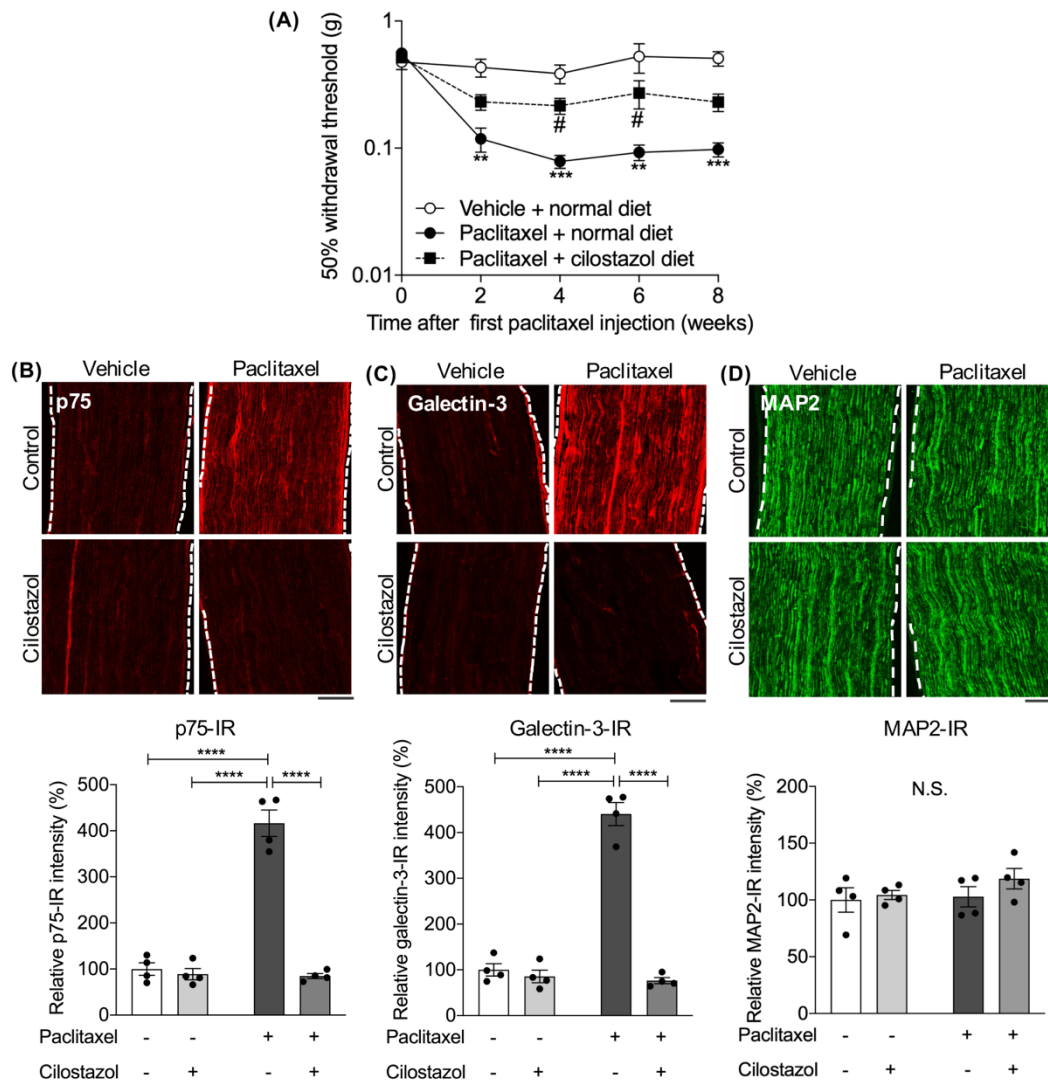


Fig. 3-6. Cilostazol prevents paclitaxel-induced mechanical hypersensitivity in mice and dedifferentiation of Schwann cells in the sciatic nerve. Mice were i.p. injected with vehicle (4.3% ethanol) or paclitaxel (5 mg/kg) twice a week for 2–8 weeks. The mice were fed a diet containing 0.3% cilostazol continuously from 1 day before the first paclitaxel injection until just before sample collection. **(A)** Time-course of changes in paw withdrawal threshold in response to mechanical stimuli in the right hindpaw. $n = 6–10$. Data are means \pm S.E.M. $**p < 0.01$ and $***p < 0.001$ vs. vehicle + normal diet; $\#p < 0.05$ vs. paclitaxel + normal diet. **(B, C, D)** Representative fluorescence micrographs (upper panels) and quantification of intensity (lower graphs) of p75-, galectin-3-, or MAP2-IR within longitudinal sections of the sciatic nerve 2 weeks after the first injection. Scale bars: 100 μ m. $n = 4$. Data are expressed relative to the value in vehicle + normal diet groups (% of control) and are represented as means \pm S.E.M. $**p < 0.01$, and $***p < 0.001$. N.S.: not significant.

Cilostazol suppresses paclitaxel-induced mechanical hypersensitivity by inhibition of Schwann cell dedifferentiation

I then investigated whether cilostazol could attenuate paclitaxel-induced mechanical hypersensitivity. CIPN model mice were generated by repeated injection of paclitaxel (5 mg/kg, i.p.) twice a week (on days 1 and 2) for 8 weeks. Measurement of 50% withdrawal

threshold was conducted on day 7 of weeks 2, 4, 6, and 8. According to the method of continuous oral dosing of cilostazol used in previous studies (77,78), mice were fed a diet containing 0.3% cilostazol continuously from 1 day before the first paclitaxel injection until just before sample collection. During the experimental period, average daily food intake was 2.86–4.62 g/mouse, without substantial difference between the treatment groups. The estimated daily cilostazol dosage was 425–480 mg/kg, which is reasonable as previous studies showed that oral administration of cilostazol to mice at doses up to 1000 mg/kg had little effect on their general behavior (82). Repeated injection of paclitaxel for 2 weeks significantly lowered the 50% threshold for hindpaw withdrawal from mechanical stimuli compared to vehicle (4.2% ethanol) injection, and the effect lasted for 8 weeks. By contrast, continuous oral administration of cilostazol reduced paclitaxel-induced mechanical hypersensitivity from 2 to 8 weeks after paclitaxel injection significantly at 4 and 6 weeks after the first injection (Fig. 3-6A). I did not observe significant differences in the 50% withdrawal threshold between the paclitaxel+cilostazol-containing diet group and the vehicle+normal diet group. Under these conditions, p75- and galectin-3-IRs were significantly elevated within longitudinal sections of the sciatic nerve obtained from mice that received normal diet and paclitaxel at 2 weeks after the first paclitaxel injection. These changes were significantly inhibited by a cilostazol-containing diet (Fig. 3-6B and C). I did not observe differences between the groups in MAP2-positive neural axons in the sciatic nerve 2 weeks after paclitaxel or vehicle injection (Fig. 3-6D).

Cilostazol does not interfere paclitaxel-induced anti-cancer effect

Finally, to determine whether cilostazol interferes with the anti-cancer effect of paclitaxel, I conducted MTT assays using the human breast cancer cell line MDA-MB-231.

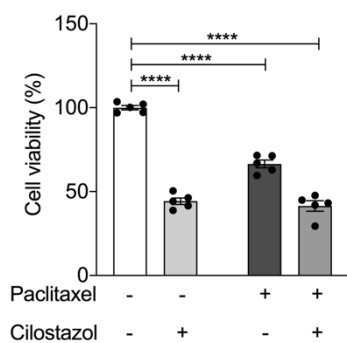


Fig. 3-7. Cilostazol does not block the anti-cancer effect of paclitaxel. Viability of breast cancer cell line, MDA-MB-231, 48 h after exposure to vehicle (0.1% DMSO) or paclitaxel (10 nM) in the absence or presence of cilostazol (30 μ M). $n = 5$. Data are expressed relative to the value in vehicle-treated cells (% of control) and are represented as means \pm S.E.M. * $p < 0.05$, ** $p < 0.01$.

Treatment with paclitaxel (10 nM) for 48 h significantly decreased the viability of MDA-MB-231 cells (Fig. 3-7). Consistent with a previous report (83), cilostazol (30 μ M) also significantly decreased the viability of these cells. However, co-treatment with cilostazol did not affect the anti-cancer effect of paclitaxel on MDA-MB-231.

Discussion

In the present study, I showed for the first time that the PDE3 inhibitor cilostazol reduces mechanical hypersensitivity in paclitaxel-related CIPN model mice by a mechanism involving cAMP/Epac-mediated Schwann cell differentiation. Therefore, I propose that cilostazol and other PDE inhibitors could be used as novel causal therapeutics to alleviate exacerbation of paclitaxel-related CIPN.

To overcome CIPN, a paradigm shift from conventional symptomatic therapies to treatments that directly address the root of CIPN is still needed. In Chapters 1 and 2, I demonstrated that Schwann cell dedifferentiation and the resultant demyelination underlie paclitaxel-induced CIPN. In this chapter, I revealed that these dedifferentiated Schwann cells spontaneously reverted to a mature state after removal of paclitaxel, suggesting that Schwann cells retain the ability to differentiate even after the paclitaxel treatment. Therefore, I hypothesized that a drug that facilitates Schwann cell redifferentiation or prevents paclitaxel-induced Schwann cell dedifferentiation could serve as a novel causal therapy for paclitaxel-related CIPN. Based on reports that accumulation of intracellular cAMP promotes Schwann cell differentiation (75,84), I attempted to identify a PDE inhibitor that could increase the level of intracellular cAMP in Schwann cells.

Among the representative PDE inhibitors that I screened, cilostazol was found to potently induce Schwann cell differentiation. In addition, I found that Epac, a major downstream effector of cAMP, is involved in cilostazol-induced differentiation of immature Schwann cells. These findings are in agreement with previous reports showing that cAMP/Epac signaling, but not the cAMP/PKA pathway, is an important determinant for initiating the Schwann cell differentiation program (75,84). Like cilostazol, Schwann cell differentiation was also induced by the PDE5 inhibitor sildenafil, which increases the levels of both cAMP and cyclic guanosine monophosphate (cGMP) (85,86). The terminal elimination half-lives of cilostazol and sildenafil in human blood are approximately 10

and 3 h, respectively (79,87). Therefore, I selected cilostazol as the primary candidate drug in this study because a longer half-life in the blood would be more appropriate in the context of treating CIPN, which has lasting symptoms, such as paresthesia, dysesthesia, and numbness. On the other hand, although benztropine has been proposed as a novel MS therapeutic candidate with the ability to differentiate OPCs (72), I observed no effect of benztropine on Schwann cell differentiation. The results suggest that the differentiation processes of Schwann cells and oligodendrocytes in the nervous system are regulated by different mechanisms.

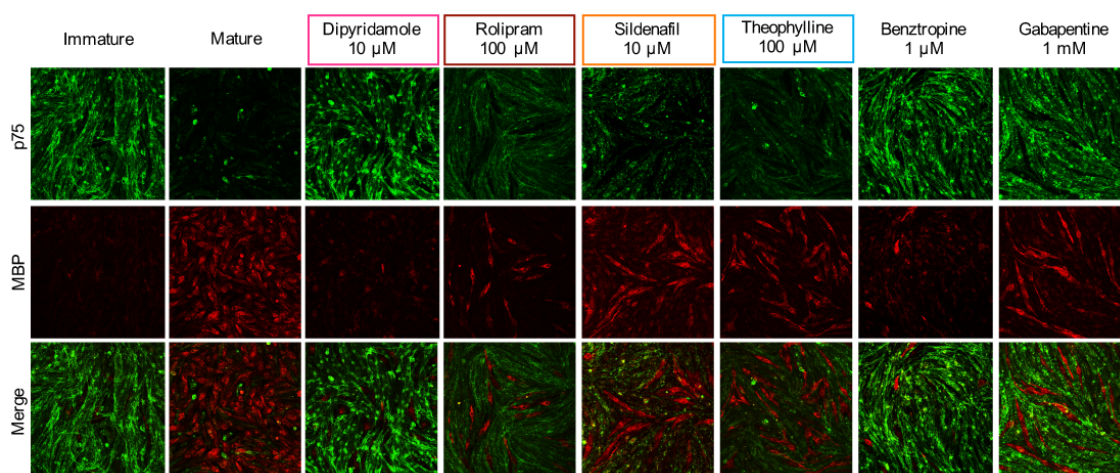
The key finding in this study is that cilostazol almost completely inhibited paclitaxel-induced Schwann cell dedifferentiation, accompanied by elevated expression of p75/galectin-3 and reduced expression of MBP. As shown in Chapter 1, paclitaxel decreased the abundance of myelin-forming Schwann cells in Schwann cell/DRG neuron co-cultures without affecting the MAP-2-positive neuronal axis. Paclitaxel-induced demyelination was abolished by co-treatment with cilostazol. Notably, cilostazol prevented p75/galectin-3 upregulation in Schwann cells within the sciatic nerve, as well as the development of mechanical hypersensitivity in paclitaxel-induced CIPN model mice. Thus, my study provides proof of concept that cilostazol, which facilitates cAMP/Epac-dependent Schwann cell differentiation, has potential as a causal therapeutic for paclitaxel-related CIPN associated with demyelination.

Cilostazol has a wide range of pharmacological actions, including antiplatelet, antithrombotic, vasodilatory, and anti-inflammatory effects, and is used in clinic to improve the symptoms of intermittent claudication in peripheral vascular diseases (80,88,89). In addition, preclinical studies have shown that cilostazol prevents the development of diabetic neuropathy, although the efficacy has not been proven in clinical trials (90). This effect of cilostazol on diabetic neuropathy is thought to be mediated by improvement of nerve conduction velocity (91,92) and nerve blood flow (93,94). Hence, the present study does not exclude the possibility that the beneficial effect of cilostazol on paclitaxel-related CIPN may be due to the diverse actions described above. Nonetheless, given the direct effect of cilostazol on primary cultured Schwann cells, my data emphasize that cilostazol is a candidate CIPN therapeutic with a novel mechanism. On the other hand, I found that cilostazol only partially alleviated mechanical hypersensitivity in CIPN mice. It is widely accepted that pathological changes in sensory neurons due to neurotoxicity are also responsible for taxane-related CIPN (66). Taken

together with my findings, I speculate that both decreasing the neurotoxicity of paclitaxel and promoting Schwann cell differentiation may be necessary to completely suppress paclitaxel-related CIPN.

The clinical benefit of cilostazol as a treatment for paclitaxel-related CIPN was further reinforced by present MTT assays in the human breast cancer cell line MDA-MB-231. Generally, paclitaxel blocks progression of cancer cell mitosis, resulting in apoptosis (95). Conveniently, inhibition of PDE facilitates apoptosis and cell-cycle arrest in cancer cells via elevation of cAMP or cGMP levels (83). In fact, cilostazol potentiated, rather than prevented, paclitaxel-induced reduction of MDA-MB-231 viability. Although these findings should be validated in future experiments using more appropriate models, such as in cancer xenograft mice, the data highlight the utility of cilostazol as a novel therapeutic that avoids the development of paclitaxel-related CIPN without compromising the anti-cancer properties of paclitaxel.

I conclude that cilostazol suppresses paclitaxel-related CIPN by facilitating Schwann cell differentiation through activation of the cAMP/Epac signaling, without impeding the anti-cancer effect of paclitaxel.



Supplemental Fig. 3-1. Effects of candidate drugs on the differentiation state of primary cultured Schwann cells. Representative confocal micrographs showing p75 (green) and MBP (red) in primary cultures of rat Schwann cells. Immature Schwann cells were treated for 48 h with vehicle-containing maintenance medium as a negative control (immature Schwann cells), vehicle-containing differentiation medium as a positive control (mature Schwann cells), or the indicated drugs diluted in maintenance medium at the final concentration indicated in the figures.

Summary

In this study, I investigated the mechanism underlying taxane-induced CIPN pathogenesis and explored a novel causal therapy for CIPN, focusing on Schwann cells. I made the following findings.

In Chapter 1, I demonstrated that taxanes induce dedifferentiation of Schwann cells prior to impairment of sensory neurons. It seems that this direct effect on Schwann cells caused by taxanes may disrupt cross talk between myelin-forming mature Schwann cells and neural axons, thereby promoting peripheral neuropathy.

In Chapter 2, I found that elevation of the plasma galectin-3 level is a CIPN-related pathological change common to humans and mice treated with taxanes. The increased plasma galectin-3 is likely to be derived from taxane-induced dedifferentiated Schwann cells. Galectin-3-dependent macrophage infiltration into the peripheral nerves could be involved in the early phase, rather than the late phase, of taxane-induced mechanical hypersensitivity in a mouse model of CIPN.

In Chapter 3, I revealed that PDE3 inhibitor cilostazol induce Schwann cell differentiation via cAMP/Epac signaling. Cilostazol suppressed paclitaxel-induced Schwann cell dedifferentiation and mechanical hypersensitivity in a mouse model of paclitaxel-related CIPN. Cilostazol did not impede the anti-cancer effect of paclitaxel on the breast cancer cell line. Thus, cilostazol could be a novel causal therapeutic to prevent development of paclitaxel-related CIPN.

Overall, the present study showed that galectin-3 secreted from taxane-induced dedifferentiated Schwann cells plays a pro-nociceptive roll via macrophage infiltration and participates in the development of CIPN. Furthermore, cilostazol, an approved antiplatelet drug, could be easily applied to medication for CIPN. These findings raise the possibility that a drug that facilitates Schwann cell differentiation and myelination could be used as a causal therapy for taxane-related CIPN and might also give a novel strategy for management of other demyelinating peripheral neuropathies.

Acknowledgements

I would like to express my profound gratitude to Professor Kazuo Matsubara (Department of Clinical Pharmacology and Therapeutics, Kyoto University Hospital; Department of Pharmacy, Wakayama University Hospital) for his kind guidance, valuable suggestions and supports.

I am deeply grateful to Dr. Satoshi Imai (Department of Clinical Pharmacology and Therapeutics, Kyoto University Hospital) for his lots of kind supports, and instructive guidance and suggestions on experimental designs, techniques, and writing papers.

I would like to express my sincere thanks to Dr. Takayuki Nakagawa, Dr. Atsushi Yonezawa, Dr. Shunsaku Nakagawa and Mr. Kotaro Itohara (Department of Clinical Pharmacology and Therapeutics, Kyoto University Hospital), Dr. Tomohiro Omura (Department of Pharmacy, Kobe University Hospital), and Dr. Yuki Sato (Department of Pharmacokinetics, Faculty of Pharmaceutical Sciences, Hokkaido University) for their kind and valuable suggestions and discussions.

I am sincerely grateful to Dr. Nobuko Kawaguchi-Sakita and Dr. Takeshi Kotake (Department of Breast Surgery, Kyoto University Hospital), and Ms. Yoko Iguma (Department of Clinical Pharmacology and Therapeutics, Kyoto University Hospital) for their kindly recruiting the patients for the clinical study and their helpful suggestions and discussions. I also thank BORN (Breast Oncology Research Network) BioBank, and all the participants in this study.

I would like to express my sincere gratitude to Dr. Toshiyuki Araki and Shuji Wakatsuki (Department of peripheral nervous System Research, National Institute of Neuroscience) for their kindly teaching me experimental techniques on primary DRG explant cultures and Schwann cell cultures.

I am deeply grateful to Professor Shuji Kaneko, Dr. Hisashi Shiralawa and Dr. Kazuki Nagayasu (Department of Molecular Pharmacology, Graduate School of Pharmaceutical Sciences, Kyoto University) for their valuable advice and technical supports on gene-editing experiments.

I deeply thanks to Dr. Takahito Miyake, Dr. Kanako So, Dr. Koichi Isami and Mr. Ziauddin Azimi (Graduate School of Pharmaceutical Sciences, Kyoto University) for their helpful advices on experimental techniques.

I would like to thank Dr. Takashi Ogihara, Mr. Ntogwa Mpumelelo, Ms. Yui Nakazato, Ms. Mayuna Matsumoto, Ms. Ren Hiraiwa, Mr. Yuki Iwamitsu, Ms. Mamiko Saigo, Ms. Akari Moriya and all other members of Department of Clinical Pharmacology and Therapeutics, Kyoto University Hospital, for their kind support.

I would like to thank the Japan Society for the Promotion of Science (JSPS) for financial support.

Finally, I thank my parents, Yoshimichi and Tomoko for their understanding and warm and constant encouragement.

List of Publications

1. Taxanes and platinum derivatives impair Schwann cells via distinct mechanisms

Satoshi Imai[#], Madoka Koyanagi[#], Ziauddin Azimi[#], Yui Nakazato, Mayuna Matsumoto, Takashi Ogihara, Atsushi Yonezawa, Tomohiro Omura, Shunsaku Nakagawa, Shuji Wakatsuki, Toshiyuki Araki, Shuji Kaneko, Takayuki Nakagawa, Kazuo Matsubara (# equally contributed)

Scientific Reports. **2017**;7:5947

DOI: 10.1038/s41598-017-05784-1

2. Pro-nociceptive roles of Schwann cell-derived galectin-3 in taxane-induced peripheral neuropathy

Madoka Koyanagi, Satoshi Imai, Mayuna Matsumoto, Yoko Iguma, Nobuko Kawaguchi-Sakita, Takeshi Kotake, Yuki Iwamitsu, Mpumelelo Ntogwa, Ren Hiraiwa, Kazuki Nagayasu, Mamiko Saigo, Takashi Ogihara, Atsushi Yonezawa, Tomohiro Omura, Shunsaku Nakagawa, Takayuki Nakagawa, Kazuo Matsubara

Cancer Research. **2021**;81:2207-2219

DOI: 10.1158/0008-5472.CAN-20-2799

3. Cilostazol is an effective causal therapy for preventing paclitaxel-induced peripheral neuropathy by suppression of Schwann cell dedifferentiation

Madoka Koyanagi, Satoshi Imai, Yuki Iwamitsu, Mayuna Matsumoto, Mamiko Saigo, Akari Moriya, Takashi Ogihara, Yui Nakazato, Atsushi Yonezawa, Shunsaku Nakagawa, Takayuki Nakagawa, Kazuo Matsubara

Neuropharmacology. **2021**;188:108514

DOI: 10.1016/j.neuropharm.2021.108514

References

1. Seretny M, Currie GL, Sena ES, Ramnarine S, Grant R, MacLeod MR, *et al.* Incidence, prevalence, and predictors of chemotherapy-induced peripheral neuropathy: A systematic review and meta-analysis. *Pain* **2014**;155:2461-70
2. Velasco R, Bruna J. Taxane-Induced Peripheral Neurotoxicity. *Toxics* **2015**;3:152-69
3. Wilkes G. Peripheral neuropathy related to chemotherapy. *Semin Oncol Nurs* **2007**;23:162-73
4. Hausheer FH, Schilsky RL, Bain S, Berghorn EJ, Lieberman F. Diagnosis, management, and evaluation of chemotherapy-induced peripheral neuropathy. *Semin Oncol* **2006**;33:15-49
5. Melli G, Jack C, Lambrinos GL, Ringkamp M, Höke A. Erythropoietin protects sensory axons against paclitaxel-induced distal degeneration. *Neurobiol Dis* **2006**;24:525-30
6. Leandro-García LJ, Leskelä S, Jara C, Gréen H, Avall-Lundqvist E, Wheeler HE, *et al.* Regulatory polymorphisms in β -tubulin IIa are associated with paclitaxel-induced peripheral neuropathy. *Clin Cancer Res* **2012**;18:4441-8
7. LaPointe NE, Morfini G, Brady ST, Feinstein SC, Wilson L, Jordan MA. Effects of eribulin, vincristine, paclitaxel and ixabepilone on fast axonal transport and kinesin-1 driven microtubule gliding: implications for chemotherapy-induced peripheral neuropathy. *Neurotoxicology* **2013**;37:231-9
8. Dorsey SG, Kleckner IR, Barton D, Mustian K, O'Mara A, St Germain D, *et al.* The National Cancer Institute Clinical Trials Planning Meeting for Prevention and Treatment of Chemotherapy-Induced Peripheral Neuropathy. *J Natl Cancer Inst* **2019**;111:531-7
9. Hu S, Huang KM, Adams EJ, Loprinzi CL, Lustberg MB. Recent Developments of Novel Pharmacologic Therapeutics for Prevention of Chemotherapy-Induced Peripheral Neuropathy. *Clin Cancer Res* **2019**;25:6295-301
10. Stubblefield MD, Burstein HJ, Burton AW, Custodio CM, Deng GE, Ho M, *et al.* NCCN task force report: management of neuropathy in cancer. *J Natl Compr Cancer Netw* **2009**;7 Suppl 5:S1-S26; quiz S7-8
11. Røyttä M, Raine CS. Taxol-induced neuropathy: chronic effects of local injection.

- J Neurocytol **1986**;15:483-96
12. Flatters SJ, Bennett GJ. Studies of peripheral sensory nerves in paclitaxel-induced painful peripheral neuropathy: evidence for mitochondrial dysfunction. *Pain* **2006**;122:245-57
 13. Polomano RC, Mannes AJ, Clark US, Bennett GJ. A painful peripheral neuropathy in the rat produced by the chemotherapeutic drug, paclitaxel. *Pain* **2001**;94:293-304
 14. Siau C, Xiao W, Bennett GJ. Paclitaxel- and vincristine-evoked painful peripheral neuropathies: loss of epidermal innervation and activation of Langerhans cells. *Exp Neurol* **2006**;201:507-14
 15. Jessen KR, Mirsky R. The origin and development of glial cells in peripheral nerves. *Nat Rev Neurosci* **2005**;6:671-82
 16. Chen ZL, Yu WM, Strickland S. Peripheral regeneration. *Annu Rev Neurosci* **2007**;30:209-33
 17. Rotshenker S. Wallerian degeneration: the innate-immune response to traumatic nerve injury. *J Neuroinflammation* **2011**;8
 18. Saitoh F, Araki T. Proteasomal degradation of glutamine synthetase regulates schwann cell differentiation. *J Neurosci* **2010**;30:1204-12
 19. Nagai T, Ibata K, Park ES, Kubota M, Mikoshiba K, Miyawaki A. A variant of yellow fluorescent protein with fast and efficient maturation for cell-biological applications. *Nat Biotech* **2002**;20:87-90
 20. Farhadi HF, Lepage P, Forghani R, Friedman HC, Orfali W, Jasmin L, *et al.* A combinatorial network of evolutionarily conserved myelin basic protein regulatory sequences confers distinct glial-specific phenotypes. *J Neurosci* **2003**;23:10214-23
 21. Nishitani N, Nagayasu K, Asaoka N, Yamashiro M, Andoh C, Nagai Y, *et al.* Manipulation of dorsal raphe serotonergic neurons modulates active coping to inescapable stress and anxiety-related behaviors in mice and rats. *Neuropsychopharmacology* **2019**;44:721-32
 22. So K, Haraguchi K, Asakura K, Isami K, Sakimoto S, Shirakawa H, *et al.* Involvement of TRPM2 in a wide range of inflammatory and neuropathic pain mouse models. *J Pharmacol Sci* **2015**;127:237-43
 23. Callahan BL, Gil AS, Levesque A, Mogil JS. Modulation of mechanical and

- thermal nociceptive sensitivity in the laboratory mouse by behavioral state. *J Pain* **2008**;9:174-84
24. Chaplan SR, Bach FW, Pogrel JW, Chung JM, Yaksh TL. Quantitative assessment of tactile allodynia in the rat paw. *J Neurosci Methods* **1994**;53:55-63
 25. Woodhoo A, Sommer L. Development of the Schwann cell lineage: from the neural crest to the myelinated nerve. *Glia* **2008**;56:1481-90
 26. Liu Z, Jin Y-Q, Chen L, Wang Y, Yang X, Cheng J, *et al.* Specific Marker Expression and Cell State of Schwann Cells during Culture In Vitro. *PLOS ONE* **2015**;10:e0123278
 27. Niapour A, Karamali F, Karbalaie K, Kiani A, Mardani M, Nasr-Esfahani MH, *et al.* Novel method to obtain highly enriched cultures of adult rat Schwann cells. *Biotechnol Lett* **2010**;32:781-6
 28. Pietrucha-Duteczakv M, Marcol W, Francuz T, Gołka D, Lewin-Kowalik J. A new protocol for cultivation of predegenerated adult rat Schwann cells. *Cell Tissue Bank* **2014**;15:403-11
 29. Huizing MT, Giaccone G, van Warmerdam LJ, Rosing H, Bakker PJ, Vermorken JB, *et al.* Pharmacokinetics of paclitaxel and carboplatin in a dose-escalating and dose-sequencing study in patients with non-small-cell lung cancer. *J Clin Oncol* **1997**;15:317-29
 30. Hao W, Tashiro S, Hasegawa T, Sato Y, Kobayashi T, Tando T, *et al.* Hyperglycemia Promotes Schwann Cell De-differentiation and De-myelination via Sorbitol Accumulation and Igf1 Protein Down-regulation. *J Biol Chem* **2015**;290:17106-15
 31. Krajewski KM, Lewis RA, Fuerst DR, Turansky C, Hinderer SR, Garbern J, *et al.* Neurological dysfunction and axonal degeneration in Charcot-Marie-Tooth disease type 1A. *Brain* **2000**;123 (Pt 7):1516-27
 32. Chentanez V, Sanguanrungririgul S, Panyasawad N. Effects of ganglioside on paclitaxel (Taxol) induced neuropathy in rats. *J Med Assoc Thai* **2003**;86:449-56
 33. Leandri M, Ghignotti M, Emionite L, Leandri S, Cilli M. Electrophysiological features of the mouse tail nerves and their changes in chemotherapy induced peripheral neuropathy (CIPN). *J Neurosci Methods* **2012**;209:403-9
 34. Stubblefield MD, Vahdat LT, Balmaceda CM, Troxel AB, Hesdorffer CS, Gooch CL. Glutamine as a neuroprotective agent in high-dose paclitaxel-induced

- peripheral neuropathy: a clinical and electrophysiologic study. *Clin Oncol* **2005**;17:271-6
35. Shin YH, Lee SJ, Jung J. Extracellular ATP inhibits Schwann cell dedifferentiation and proliferation in an ex vivo model of Wallerian degeneration. *Biochem Biophys Res Commun* **2013**;430:852-7
 36. Taniuchi M, Clark HB, Schweitzer JB, Johnson EM. Expression of nerve growth factor receptors by Schwann cells of axotomized peripheral nerves: ultrastructural location, suppression by axonal contact, and binding properties. *J Neurosci* **1988**;8:664
 37. Jung J, Cai W, Jang SY, Shin YK, Suh DJ, Kim JK, *et al.* Transient lysosomal activation is essential for p75 nerve growth factor receptor expression in myelinated Schwann cells during Wallerian degeneration. *Anat Cell Biol* **2011**;44:41-9
 38. Reichert F, Saada A, Rotshenker S. Peripheral nerve injury induces Schwann cells to express two macrophage phenotypes: phagocytosis and the galactose-specific lectin MAC-2. *J Neurosci* **1994**;14:3231-45
 39. Nobusue H, Onishi N, Shimizu T, Sugihara E, Oki Y, Sumikawa Y, *et al.* Regulation of MKL1 via actin cytoskeleton dynamics drives adipocyte differentiation. *Nat Commun* **2014**;5:3368
 40. Domic J, Dabelic S, Flogel M. Galectin-3: an open-ended story. *Biochim Biophys Acta* **2006**;1760:616-35
 41. Chen A, Hou W, Zhang Y, Chen Y, He B. Prognostic value of serum galectin-3 in patients with heart failure: a meta-analysis. *Int J Cardiol* **2015**;182:168-70
 42. Ghorbani A, Bhambhani V, Christenson RH, Meijers WC, de Boer RA, Levy D, *et al.* Longitudinal Change in Galectin-3 and Incident Cardiovascular Outcomes. *J Am Coll Cardiol* **2018**;72:3246-54
 43. Li S, Li S, Hao X, Zhang Y, Deng W. Perindopril and a Galectin-3 Inhibitor Improve Ischemic Heart Failure in Rabbits by Reducing Gal-3 Expression and Myocardial Fibrosis. *Front Physiol* **2019**;10:267
 44. Boza-Serrano A, Ruiz R, Sanchez-Varo R, Garcia-Revilla J, Yang Y, Jimenez-Ferrer I, *et al.* Galectin-3, a novel endogenous TREM2 ligand, detrimentally regulates inflammatory response in Alzheimer's disease. *Acta Neuropathol* **2019**;138:251-73

45. Ntogwa M, Imai S, Hiraiwa R, Koyanagi M, Matsumoto M, Ogihara T, *et al.* Schwann cell-derived CXCL1 contributes to human immunodeficiency virus type 1 gp120-induced neuropathic pain by modulating macrophage infiltration in mice. *Brain Behav Immun* **2020**; 88:325-39
46. Isami K, Imai S, Sukeishi A, Nagayasu K, Shirakawa H, Nakagawa T, *et al.* The impact of mouse strain-specific spatial and temporal immune responses on the progression of neuropathic pain. *Brain Behav Immun* **2018**;74:121-32
47. Langer CJ, Stephenson P, Thor A, Vangel M, Johnson DH. Trastuzumab in the treatment of advanced non-small-cell lung cancer: is there a role? Focus on Eastern Cooperative Oncology Group study 2598. *J Clin Oncol* **2004**;22:1180-7
48. Krop IE, Modi S, LoRusso PM, Pegram M, Guardino E, Althaus B, *et al.* Phase 1b/2a study of trastuzumab emtansine (T-DM1), paclitaxel, and pertuzumab in HER2-positive metastatic breast cancer. *Breast Cancer Res* **2016**;18:34
49. Zielinski C, Lang I, Inbar M, Kahan Z, Greil R, Beslija S, *et al.* Bevacizumab plus paclitaxel versus bevacizumab plus capecitabine as first-line treatment for HER2-negative metastatic breast cancer (TURANDOT): primary endpoint results of a randomised, open-label, non-inferiority, phase 3 trial. *Lancet Oncol* **2016**;17:1230-9
50. van Rossum AGJ, Kok M, van Werkhoven E, Opdam M, Mandjes IAM, van Leeuwen-Stok AE, *et al.* Adjuvant dose-dense doxorubicin-cyclophosphamide versus docetaxel-doxorubicin-cyclophosphamide for high-risk breast cancer: First results of the randomised MATADOR trial (BOOG 2004-04). *Eur J Cancer* **2018**;102:40-8
51. Wang L, Guo XL. Molecular regulation of galectin-3 expression and therapeutic implication in cancer progression. *Biomedicine Pharmacother* **2016**;78:165-71
52. Ehrhardt C, Rückle A, Hrinčius ER, Haasbach E, Anhlan D, Ahmann K, *et al.* The NF-κB inhibitor SC75741 efficiently blocks influenza virus propagation and confers a high barrier for development of viral resistance. *Cell Microbiol* **2013**;15:1198-211
53. Sano H, Hsu DK, Yu L, Apgar JR, Kuwabara I, Yamanaka T, *et al.* Human galectin-3 is a novel chemoattractant for monocytes and macrophages. *J Immunol* **2000**;165:2156-64
54. Lobry T, Miller R, Nevo N, Rocca CJ, Zhang J, Catz SD, *et al.* Interaction between

- galectin-3 and cystinosis uncovers a pathogenic role of inflammation in kidney involvement of cystinosis. *Kidney Int* **2019**;96:350-62
55. Van Rooijen N, Sanders A. Liposome mediated depletion of macrophages: mechanism of action, preparation of liposomes and applications. *J Immunol Methods* **1994**;174:83-93
 56. Stegmayr J, Zetterberg F, Carlsson MC, Huang X, Sharma G, Kahl-Knutson B, *et al.* Extracellular and intracellular small-molecule galectin-3 inhibitors. *Sci Rep* **2019**;9:2186
 57. Thijssen VL, Heusschen R, Caers J, Griffioen AW. Galectin expression in cancer diagnosis and prognosis: A systematic review. *Biochim Biophys Acta* **2015**;1855:235-47
 58. Tian J, Yang G, Chen HY, Hsu DK, Tomilov A, Olson KA, *et al.* Galectin-3 regulates inflammasome activation in cholestatic liver injury. *FASEB J* **2016**;30:4202-13
 59. Piek A, Du W, de Boer RA, Sillje HHW. Novel heart failure biomarkers: why do we fail to exploit their potential? *Crit Rev Clin Lab Sci* **2018**;55:246-63
 60. Be'eri H, Reichert F, Saada A, Rotshenker S. The cytokine network of wallerian degeneration: IL-10 and GM-CSF. *Eur J Neurosci* **1998**;10:2707-13
 61. Huang ZZ, Li D, Liu CC, Cui Y, Zhu HQ, Zhang WW, *et al.* CX3CL1-mediated macrophage activation contributed to paclitaxel-induced DRG neuronal apoptosis and painful peripheral neuropathy. *Brain Behav Immun* **2014**;40:155-65
 62. Zhang H, Li Y, de Carvalho-Barbosa M, Kavelaars A, Heijnen CJ, Albrecht PJ, *et al.* Dorsal Root Ganglion Infiltration by Macrophages Contributes to Paclitaxel Chemotherapy-Induced Peripheral Neuropathy. *J Pain* **2016**;17:775-86
 63. Biswas SK, Mantovani A. Macrophage plasticity and interaction with lymphocyte subsets: cancer as a paradigm. *Nat Immunol* **2010**;11:889-96
 64. Ren K, Dubner R. Interactions between the immune and nervous systems in pain. *Nat Med* **2010**;16:1267-76
 65. Lee WJ, Tateya S, Cheng AM, Rizzo-DeLeon N, Wang NF, Handa P, *et al.* M2 Macrophage Polarization Mediates Anti-inflammatory Effects of Endothelial Nitric Oxide Signaling. *Diabetes* **2015**;64:2836-46
 66. Peters CM, Jimenez-Andrade JM, Kuskowski MA, Ghilardi JR, Mantyh PW. An evolving cellular pathology occurs in dorsal root ganglia, peripheral nerve and

- spinal cord following intravenous administration of paclitaxel in the rat. *Brain Res* **2007**;1168:46-59
67. Abdel-Rahman O. Outcomes of early-stage breast cancer patients treated with sequential anthracyclines-taxanes in relationship to relative dosing intensity: a secondary analysis of a randomized controlled trial. *Clin Transl Oncol* **2019**;21:239-45
 68. Olawaiye AB, Java JJ, Krivak TC, Friedlander M, Mutch DG, Glaser G, *et al.* Does adjuvant chemotherapy dose modification have an impact on the outcome of patients diagnosed with advanced stage ovarian cancer? An NRG Oncology/Gynecologic Oncology Group study. *Gynecol Oncol* **2018**;151:18-23
 69. Hershman DL, Lacchetti C, Dworkin RH, Lavoie Smith EM, Bleeker J, Cavaletti G, *et al.* Prevention and management of chemotherapy-induced peripheral neuropathy in survivors of adult cancers: American Society of Clinical Oncology clinical practice guideline. *J Clin Oncol* **2014**;32:1941-67
 70. Smith EM, Pang H, Cirrincione C, Fleishman S, Paskett ED, Ahles T, *et al.* Effect of duloxetine on pain, function, and quality of life among patients with chemotherapy-induced painful peripheral neuropathy: a randomized clinical trial. *JAMA* **2013**;309:1359-67
 71. Franklin RJM, Ffrench-Constant C. Regenerating CNS myelin - from mechanisms to experimental medicines. *Nat Rev Neurosci* **2017**;18:753-69
 72. Deshmukh VA, Tardif V, Lyssiotis CA, Green CC, Kerman B, Kim HJ, *et al.* A regenerative approach to the treatment of multiple sclerosis. *Nature* **2013**;502:327-32
 73. Mei F, Fancy SPJ, Shen YA, Niu J, Zhao C, Presley B, *et al.* Micropillar arrays as a high-throughput screening platform for therapeutics in multiple sclerosis. *Nat Med* **2014**;20:954-60
 74. Najm FJ, Madhavan M, Zaremba A, Shick E, Karl RT, Factor DC, *et al.* Drug-based modulation of endogenous stem cells promotes functional remyelination in vivo. *Nature* **2015**;522:216-20
 75. Han SH, Yun SH, Shin YK, Park HT, Park JI. Heat Shock Protein 90 is Required for cAMP-Induced Differentiation in Rat Primary Schwann Cells. *Neurochem Res* **2019**;44:2643-57
 76. Sohn EJ, Park HT, Shin YK. Exosomes derived from differentiated Schwann cells

- inhibit Schwann cell migration via microRNAs. *Neuroreport* **2020**;31:515-22
77. Hase Y, Okamoto Y, Fujita Y, Kitamura A, Nakabayashi H, Ito H, *et al.* Cilostazol, a phosphodiesterase inhibitor, prevents no-reflow and hemorrhage in mice with focal cerebral ischemia. *Exp Neurol* **2012**;233:523-33
 78. Oyama N, Yagita Y, Kawamura M, Sugiyama Y, Terasaki Y, Omura-Matsuoka E, *et al.* Cilostazol, not aspirin, reduces ischemic brain injury via endothelial protection in spontaneously hypertensive rats. *Stroke* **2011**;42:2571-7
 79. Muirhead GJ, Wilner K, Colburn W, Haug-Pihale G, Rouviex B. The effects of age and renal and hepatic impairment on the pharmacokinetics of sildenafil. *Br J Clin Pharmacol* **2002**;53 Suppl 1:21s-30s
 80. Balinski AM, Preuss CV. Cilostazol. StatPearls. Treasure Island (FL): StatPearls Publishing; 2020.
 81. Cheng X, Ji Z, Tsalkova T, Mei F. Epac and PKA: a tale of two intracellular cAMP receptors. *Acta biochimica et biophysica Sinica* **2008**;40:651-62
 82. Shintani S, Toba Y, Suzuki S, Ninomiya S, Umezato M, Hiyama T. General pharmacological properties of cilostazol, a new antithrombotic drug. Part I: Effects on the central nervous system. *Arzneimittel-Forschung* **1985**;35:1157-62
 83. Savai R, Pullamsetti SS, Banat GA, Weissmann N, Ghofrani HA, Grimminger F, *et al.* Targeting cancer with phosphodiesterase inhibitors. *Expert Opin Investig Drugs* **2010**;19:117-31
 84. Bacallao K, Monje PV. Opposing roles of PKA and EPAC in the cAMP-dependent regulation of schwann cell proliferation and differentiation [corrected]. *PloS one* **2013**;8:e82354
 85. Schalcher C, Schad K, Brunner-La Rocca HP, Schindler R, Oechslin E, Scharf C, *et al.* Interaction of sildenafil with cAMP-mediated vasodilation in vivo. *Hypertension* **2002**;40:763-7
 86. Stief CG, Uckert S, Becker AJ, Harringer W, Truss MC, Forssmann WG, *et al.* Effects of sildenafil on cAMP and cGMP levels in isolated human cavernous and cardiac tissue. *Urology* **2000**;55:146-50
 87. Schrör K. The pharmacology of cilostazol. *Diabetes Obes Metab* **2002**;4 Suppl 2:S14-9
 88. Kim SM, Jung JM, Kim BJ, Lee JS, Kwon SU. Cilostazol Mono and Combination Treatments in Ischemic Stroke: An Updated Systematic Review and Meta-

- Analysis. Stroke **2019**;50:3503-11
89. Paronis E, Katsimpoulas M, Kadoglou NPE, Provost C, Stasinopoulou M, Spyropoulos C, *et al.* Cilostazol Mediates Immune Responses and Affects Angiogenesis During the Acute Phase of Hind Limb Ischemia in a Mouse Model. J Cardiovasc Pharmacol Ther **2020**;25:273-85
 90. Papanas N, Maltezos E. Cilostazol in diabetic neuropathy: premature farewell or new beginning? Angiology **2011**;62:605-8
 91. Kihara M, Schmelzer JD, Low PA. Effect of cilostazol on experimental diabetic neuropathy in the rat. Diabetologia **1995**;38:914-8
 92. Naka K, Sasaki H, Kishi Y, Furuta M, Sanke T, Nanjo K, *et al.* Effects of cilostazol on development of experimental diabetic neuropathy: functional and structural studies, and Na⁺ -K⁺ -ATPase acidity in peripheral nerve in rats with streptozotocin-induced diabetes. Diabetes Res Clin Pract **1995**;30:153-62
 93. Uehara K, Sugimoto K, Wada R, Yoshikawa T, Marukawa K, Yasuda Y, *et al.* Effects of cilostazol on the peripheral nerve function and structure in STZ-induced diabetic rats. J Diabetes Complications **1997**;11:194-202
 94. Yamamoto Y, Yasuda Y, Kimura Y, Komiya Y. Effects of cilostazol, an antiplatelet agent, on axonal regeneration following nerve injury in diabetic rats. Eur J Pharmacol **1998**;352:171-8
 95. Khing TM, Po WW, Sohn UD. Fluoxetine Enhances Anti-tumor Activity of Paclitaxel in Gastric Adenocarcinoma Cells by Triggering Apoptosis and Necroptosis. Anticancer Res **2019**;39:6155-63